



INSTITUT DE FRANCE
Académie des sciences

Comptes Rendus

Mécanique


Zoa Ambassa, Jean Chills Amba and Nandor Tamaskovics

Implementation of the c-phi reduction procedure in Cast3M code for calculating the stability of retaining walls in the layered backfill with strength parameters reduction by elasto-plastic finite element analysis using fields data

Volume 351 (2023), p. 485-523

Published online: 4 December 2023

<https://doi.org/10.5802/crmeca.230>

 This article is licensed under the
CREATIVE COMMONS ATTRIBUTION 4.0 INTERNATIONAL LICENSE.
<http://creativecommons.org/licenses/by/4.0/>



*Les Comptes Rendus. Mécanique sont membres du
Centre Mersenne pour l'édition scientifique ouverte*

www.centre-mersenne.org

e-ISSN : 1873-7234



History of Sciences and Ideas / *Histoire des sciences et des idées*

Implementation of the c-phi reduction procedure in Cast3M code for calculating the stability of retaining walls in the layered backfill with strength parameters reduction by elasto-plastic finite element analysis using fields data

Mise en œuvre de la procédure c-phi de réduction des paramètres de résistance dans le code Cast3M pour le calcul de la stabilité des murs de soutènement dans le remblai stratifié par analyse éléments finis elasto-plastique en utilisant les données de terrain

Zoa Ambassa^{Ⓢ,*}, a, b, Jean Chills Amba[Ⓢ], a, b and Nandor Tamaskovics^c

^a Laboratory of Energy Modeling Materials and Methods (E3M), National Higher Polytechnic School of Douala, University of Douala, P.O. Box: 2701 Douala, Cameroon

^b Department of Civil Engineering, National Higher Polytechnic School of Douala, University of Douala, Cameroon

^c TU Bergakademie Freiberg, Geotechnical Institute, Chair of Soil Mechanics and Ground Engineering, Gustav-Zeuner-Straße 1/Room 014/Rom 016, Germany

E-mails: zoa.amabassa@enspd-udo.cm (Z. Ambassa), jc.amba@enspd-udo.cm (J. C. Amba), Nandor.Tamaskovics@ifgt.tu-freiberg.de (N. Tamaskovics)

Abstract. This paper presents an implementation of the c-phi reduction procedure in the finite element code Cast3M. This procedure is first validated on a simple example of bearing capacity of a strip footing and then used to evaluate the stability factor of a geotechnical structure composed of two levels of backfill retained by

* Corresponding author.

two retaining walls, with a road built on the top of the second backfill. The results of the c - ϕ reduction procedure for the construction of first and second backfill are also compared to other analysis methods classically used in geotechnics and to the results of finite element calculations.

Résumé. Cet article présente une implémentation de la procédure de réduction c - ϕ dans le code aux éléments finis Cast3M. Cette procédure est d'abord validée sur un exemple simple de capacité portante d'une semelle filante, puis utilisée pour évaluer le facteur de stabilité d'une structure géotechnique composée de deux niveaux de remblai retenus par deux murs de soutènement, avec une route construite sur le dessus du second remblai. Les résultats de la procédure de réduction c - ϕ pour la construction du premier et du second remblai sont également comparés à d'autres méthodes d'analyse classiquement utilisées en géotechnique et aux résultats des calculs par éléments finis.

Keywords. Implementation, C - ϕ reduction procedure, Code Cast3M, Stability factor, Geotechnical structure, Finite element calculations.

Mots-clés. Mise en œuvre, Procédure de réduction c - ϕ , Code Cast3M, Facteur de stabilité, Structure géotechnique, Calculs par éléments finis.

Manuscript received 5 December 2022, revised 27 January 2023 and 12 June 2023, accepted 9 October 2023.

1. Introduction

For decades, the majority of slope stability analyses performed in practice still use traditional limit equilibrium approaches involving methods of slices that have remained essentially unchanged. This was not the outcome envisaged when Whitman and Bailey [1] set criteria for the then emerging methods to become readily accessible to all engineers. The Finite Element Method represents a powerful alternative approach for slope stability and retained wall analysis which is accurate, versatile and requires fewer *a priori* assumptions, especially, regarding the failure mechanism. Slope failure in the Finite Element model occurs “naturally” through the zones in which the shear strength of the soil is insufficient to resist the shear stresses. Elasto-plastic analysis of geotechnical problems using the Finite Element (FE) Method has been widely accepted in the research arena for many years; however, its routine use in geotechnical practice for slope and retaining stability analysis still remains limited. The reason for this lack of acceptance is not entirely clear; however, advocates of FE techniques in academe must take some responsibility. Practising engineers are often sceptical of the need for such complexity, especially in view of the poor quality of soil property data often available from routine site investigations [2–4]. Although this scepticism is often warranted, there are certain types of geotechnical problem for which the FE approach offers real benefits. The challenge for an experienced engineer is to know which kind of problem would benefit from a FE treatment and which would not. In general, linear problems such as the prediction of settlements and strains, the calculation of flow quantities due to steady seepage or the study of transient effects due to consolidation are all highly amenable to solution by Finite Elements. Traditional approaches involving charts, tables or graphical methods will often be adequate for routine problems but the Finite Elements approach may be valuable if awkward geometries or material variations are encountered which are not covered by traditional chart solutions.

The use of nonlinear analysis in routine geotechnical practice is harder to justify, because there is usually a significant increase in complexity which is more likely to require the help of a modelling specialist. Nonlinear analyses are inherently iterative in nature, because the material properties and/or the geometry of the problem are themselves a function of the “solution”. Objections to nonlinear analyses on the grounds that they require excessive computational power, however, have been largely overtaken by developments in, and falling costs of, computer hardware. Slope stability and retained wall represents an area of geotechnical analysis in which a nonlinear FE approach offers real benefits over existing methods. As this paper will show, Slope stability and retained wall analysis by elastoplastic Finite Elements is accurate, robust and simple

enough for routine use by practising engineers. Perception of the FE method as complex and potentially misleading is unwarranted and ignores the real possibility that misleading results can be obtained with conventional “slip circle” approaches. The graphical capabilities of FE programs also allow better understanding of the mechanisms of failure, simplifying the output from reams of paper to manageable graphs and plots of displacements.

The objective of this work is the development of an elasto-plastic calculation method for the prediction of the stability for the large geotechnical structures in interaction by Finite Element technique thanks to with methodological and sophisticated programming from Cast3M code. This work does not only concern the slope stability calculation, but the stability calculation of bearing capacity, overturning and sliding of the layered backfill and the retaining walls by the c - ϕ parameters reduction because it concerns several structures in interaction that encompass the failure mechanisms of the majority of geotechnical structures. The paper describes several standards in geotechnical practice of Finite Element retained wall and slope stability analysis with comparison against other solution methods, including the influence of a free surface on slope and layered backfill stability. Graphical output is included to illustrate displacements, deformations, stresses and mechanisms of failure.

2. Traditional methods of slope stability analysis

Most textbooks on soil mechanics or geotechnical engineering will include reference to several alternative methods of slope stability analysis. In a survey of equilibrium methods of slope stability analysis reported by Duncan [5], the characteristics of a large number of methods were summarized, including the ordinary method of slices [6], Bishop's Modified Method [7], force equilibrium methods (e.g. Lowe and Karafiath) [8], Janbu's generalized procedure of slices [9], Morgenstern and Price's method [10, 11] and Spencer's method [12]. Although there seems to be some consensus that Spencer's method is one of the most reliable, textbooks continue to describe the others in some detail, and the wide selection of available methods is at best confusing to the potential user. For example, the controversy was revisited by Lambe and Silva [13], who maintained that the ordinary method of slices had an undeservedly bad reputation. A difficulty with all the equilibrium methods is that they are based on the assumption that the failing soil mass can be divided into slices. This in turn necessitates further assumptions relating to side force directions between slices, with consequent implications for equilibrium. The assumption made about the side forces is one of the main characteristics that distinguishes one limit equilibrium method from another, and yet is itself an entirely artificial distinction.

3. Finite elements method for slope and retaining walls stability analysis

Duncan's review of FE analysis of slopes concentrated mainly on deformation rather than stability analysis of slopes; however, attention was drawn to some important early papers in which elasto-plastic soil models were used to assess stability. Smith and Hobbs [14] reported results of $\varphi_u = 0$ slopes and obtained reasonable agreement with Taylor's [15] charts. Zienkiewicz *et al.* [16] considered a c' , φ' slope and obtained good agreement with slip circle solutions. Griffiths [17, 18] extended this work to show reliable slope stability results over a wide range of soil properties and geometries as compared with charts of Bishop and Morgenstern [19]. Subsequent use of the FE method in slope stability analysis has added further confidence in the method [20–30]. Griffiths [20] investigate the probability of failure of a cohesive slope using both simple and more advanced probabilistic analysis tools. The influence of local averaging on the probability of failure of a test problem has been investigated. The advanced method, called the random finite element method (RFEM), uses elastoplasticity combined with random field theory. For the authors,

the RFEM method is shown to offer many advantages over traditional probabilistic slope stability techniques, because it enables slope failure to develop naturally by seeking out the most critical mechanism. Griffiths [20] reported that simplified probabilistic analysis, in which spatial variability is ignored by assuming perfect correlation, lead to unconservative estimates of the probability of failure. To avoid human error in the analyses criteria and find a unified mechanical explanation for slope instability, a criterion has been proposed by Chengya [21]. For the author, this criterion, of the stability is determined by identifying the positive or negative of the variational value. The Factor of safety of two and three dimensional slopes calculated by this criterion are compared with those calculated by other criteria. The effect of mesh size on the accuracy of the results have been analyzed. The study made by Anindita [22] proposes a comparison of Limit Equilibrium and Finite Element methods by numerical approach. The method developed by Dakshith [23] presents a numerical technique combining the scaled boundary finite element method and image-based meshing for slope stability analysis. Quad tree decomposition has been applied to simultaneously generate meshes and consider the spatial variation of material properties directly from the images through a mapping technique. The shear strength technique has been applied to evaluate the shear reduction factor of safety of the slope. Coal slopes at Yallourn open-pit mine, Victoria, Australia was considered, forming the basis of a case study to demonstrate the applicability of the method. Huang [24] extended the use of strength reduction FEM to include the effects of unsaturated transient seepage and some primary numerical results concerning the stability of an earth dam under rapid drawdown have been presented. A stability analysis performed on the Yashigou earth dam in China was conducted by Huy [25]. Factor of safety results were considered for vacuum dam, steady state water level and water level drawdown using finite element stresses method analysis to compare the Morgenstern–Price method. Jiang [26] has developed a slope stability analysis considering spatially variable shear strength parameters using a non-intrusive stochastic finite element method. Zoa [27] conducted a finite element analysis of a soft soil reinforced by an industrial nailing technique using a soft soil behavior model. He determined the main influential parameters. The probabilistic stability analysis of an earth dam by stochastic finite element method based on field data has been performed by Mouyeaux [28] for realistic prediction of the failure mechanism and seepages under this dam. Recently, a hybrid stacking ensemble approach Navid [29] for enhancing the prediction of slope stability. In this hybrid stacking ensemble, he used an artificial bee colony algorithm to find out the best combination of base classifiers (level 0) and determined a suitable meta-classifier (level 1) from a pool of 11 individual optimized machine learning algorithm. Finite element analysis was conducted in order to form the synthetic database for the training stage (150 cases) of proposed model while 107 real field slope cases were used for the testing stage. The results by the hybrid stacking ensemble were compared with that obtained by the 11 optimized machine learning. The comparisons showed that a significant improvement in the prediction ability of slope stability has been achieved by the hybrid stacking ensemble. A numerical model termed as ISR3DNMM-GPS method has been developed by Yantao [30] for factor of safety calculation and 3D failure surface determination involved in a 3D slope stability analysis. In this proposed numerical model, an improved strength reduction technique (ISRT) which can avoid unreasonable plastic zones appearing in the deep area of a slope has been implemented into 3D numerical manifold method, and improved strength reduction based 3DNMM is developed. Duncan mentions the potential for improved graphical results and reporting utilizing FE, but cautions against artificial accuracy being assumed when the input parameters themselves are so variable. Wong [31] gives a useful summary of potential sources of error in the FE modelling of slope stability. Other important contributions in this area come from the work of Sloan [32] who published the paper concerning the advances in stability analysis that combine the limit theorems of classical plasticity with finite elements to give rigorous upper and lower bounds on the failure load.

He proposed a new development, which incorporates pore water pressures in finite-element limit analysis and proposed of the new techniques for stability solutions including foundations, anchors, slopes, excavations and tunnels. Tschuchnigg [33] carried out a comparative study concerning the strength reduction method and rigorous limit analyses which are based on collapse theorems of plasticity.

Advantages of the finite element method

The advantages of a FE approach to slope stability analysis over traditional limit equilibrium methods can be summarized as follows:

- (a) No assumption needs to be made in advance about the shape or location of the failure surface. Failure occurs “naturally” through the zones within the soil mass in which the soil shear strength is unable to sustain the applied shear stresses.
- (b) Since there is no concept of slices in the FE approach, there is no need for assumptions about slice side forces. The FE method preserves global equilibrium until “failure” is reached.
- (c) If realistic soil compressibility data are available, the FE solutions will give information about deformations at working stress levels.
- (d) The FE method is able to monitor progressive failure up to and including overall shear failure.

The developments which follow in this paper, are inspired by these important contributions on this topic.

4. Methodology

After this literature review related to the problematic, the methodology adopted in this paper consists first of all in describing the site location of the geotechnical structures design on the geological and geomorphological aspects. Then the numerical modeling of the structures will be approached by first validating the program for calculating the bearing capacity and settlement of a strip footing placed on an elastoplastic soil whose analytical solutions are known. Then the numerical modeling of the problem will be compared with that other software for the same problem. The different calculation phases obeying the staged construction of these geotechnical structures will be respected in our numerical modeling. Settlements will be analyzed at the serviceability limit state and all other failure criteria at the ultimate limit state.

4.1. Presentation of the construction site of the geotechnical structures

The project site is located in the Douala city in Cameroon. It is very rugged with a steep incline. The objective is to build a series of geotechnical structures to guarantee the stability of the road whose projection from the level of the platform is at the top of slope. Figure 1 illustrates the shadings of the contour lines of the site, the position and the direction in cross-section of the geotechnical structures under investigation.

4.2. Geology of site project

In the Littoral region of Cameroon, the sedimentary rocks form low lying and gently undulating hills along the western side of the Dibamba river. The strata have experienced tropical weathering, which has resulted in the development of a lateritic residual soil profile. This type of rock

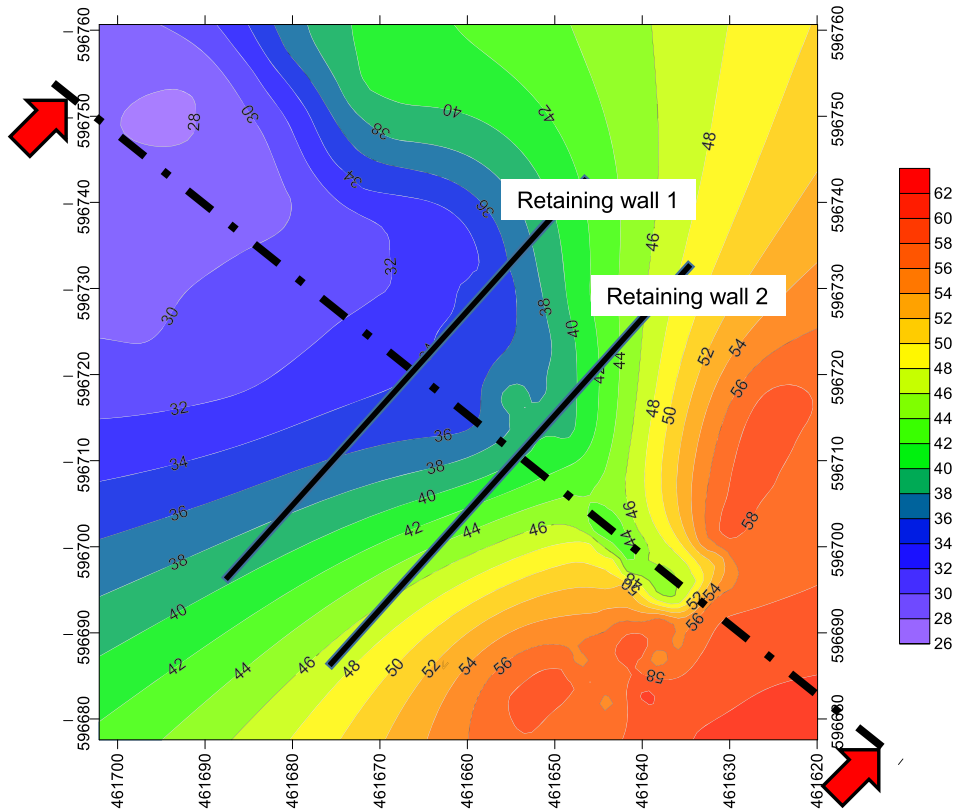


Figure 1. Shadings of the contour lines of the site, the position and the direction in cross-section of the geotechnical structures.

mass tropical leads to weathering profiles as presented by Fookes [34]. The material viewed at site comprises Weathering Grade 6, as seen in the trial pit photograph from site, with possibly weathering Grade 5 material encountered towards the base of deeper rotary boreholes [35, 36]. Below this material, the stratum may then transition more rapidly to weathered parent rock material. This transition was not identified in the deepest exploratory boreholes that went 30 m below ground level. In the exploratory holes observed there was no clear evidence for overlying transported material, so material may be weathered *in-situ*.

4.3. Behaviour laws of subsoil, basement and backfill materials

The first step of the proposed approach consists in characterizing on the one hand the behaviour of the natural materials constituting the structures whose stability is sought to be assessed by choosing an elastoplastic law to represent them, and on the other hand in estimating in a relevant way a value deterministic for each of the parameters of the constitutive law, which associated with other variables, will constitute the input data of the Finite Element model. The choice of a constitutive law depends on the mechanism to be modeled, the data available for the structures, but above all on the precision sought and numerical considerations. We are interested in the mechanisms that can lead structures under extreme stresses to failure. However, to calculate the safety factor relating to the behavior of geotechnical structures by the Finite Element Method,

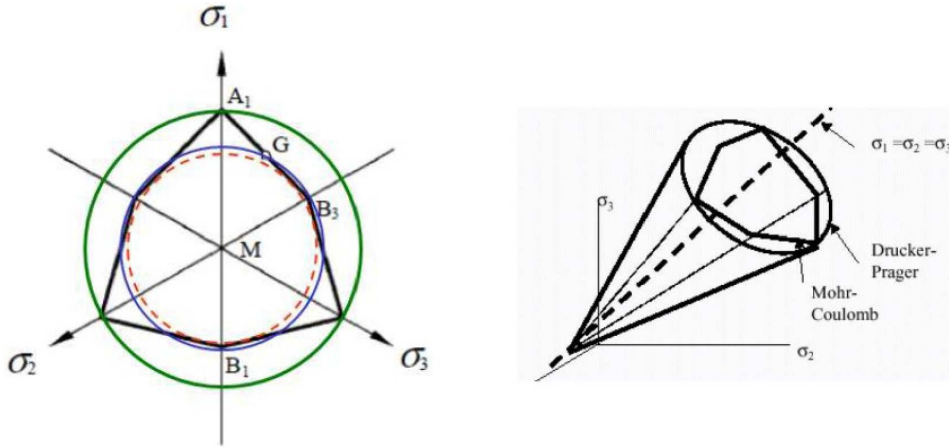


Figure 2. Mohr–Coulomb and Drucker–Prager yield criteria.

the evaluation of the elastic deformations does not matter because it is the modeling of the appearance and the evolution of the unstabilized plastic deformations which is important. Among the laws at our disposal and described in Mestat [37], we present here two classic behavior laws of the elastoplastic type: those of Mohr–Coulomb and Drucker–Prager. These two laws have the advantage of depending on few parameters directly from triaxial and oedometric tests. They allow a certain “economy” of data acquisition and management which are, in particular those concerning the mechanical characterization of materials, relatively few in number and not very varied on geotechnical projects.

The Mohr–Coulomb criterion is the first that was proposed for soils [37]. It is used for long-term for frictional and cohesive soils. It is characterized by the relations:

$$F(\sigma_{ij}) = (\sigma_1 - \sigma_3) - (\sigma_1 + \sigma_3) \sin \varphi - 2c \cos \varphi \leq 0 \tag{1}$$

$$G(\sigma_{ij}) = (\sigma_1 - \sigma_3) - (\sigma_1 + \sigma_3) \sin \psi + c^{ste} \tag{2}$$

where c is the cohesion of the material, φ is the friction angle, and ψ is the dilatancy angle. σ_1 and σ_3 represent the principal stresses ($\sigma_1 \geq \sigma_2 \geq \sigma_3$). In the principal stress space, the surface defined by the Mohr–Coulomb criterion is a hexagonal pyramid with axis ($\sigma_1 = \sigma_2 = \sigma_3$) (Figure 2b).

Analogies are possible between the Mohr–Coulomb and Drucker–Prager criteria (Figure 2). Relations can be established between the parameters (α, γ, k) and (φ, ψ, c) in certain situations [37]. The Drucker–Prager criterion is written:

$$f(\sigma) = \sqrt{J_2} + \alpha I_1 - K \leq 0 \tag{3}$$

$$f(\sigma) = \sigma_e + \sin \alpha I_1 - K' \leq 0. \tag{4}$$

The correspondence between the Mohr–Coulomb criteria and those of Drucker–Prager are as follows [37]:

$$ALFA = ETA = \frac{2\sqrt{3} \sin \varphi}{9 - \sin^2 \varphi}, \quad GAMMA = \frac{2\sqrt{3} \sin \psi}{9 - \sin^2 \psi}, \quad K = KL = \frac{6\sqrt{3}c \cdot \cos \varphi}{9 - \sin^2 \varphi}. \tag{5}$$

Moreover, the choice of a criterion must also be guided by the possible numerical difficulties of implementing the criterion. Some constitutive laws, such as that of Mohr–Coulomb for example, have a failure criterion comprising singular edges (Figure 2b), which can numerically result in

convergence difficulties [28, 38]. In view of the above, the Drucker–Prager model implemented in the Cast3M Finite Elements code will be used in this paper to describe the elastoplastic behavior of untreated materials.

4.4. Conceptual basis of the c - ϕ reduction procedure in Cast3M

The c - ϕ reduction procedure developed is used to determine the factor of safety in this part and part 5. The concept of the strength reduction method is based:

Strength reduction method—Global safety factor concept: FOS

$$R_n = \|f - K(\varphi_{k,\text{mob}}, c_{k,\text{mob}}, \psi_{k,\text{mob}}, \sigma_{t,\text{mob}}) \cdot u_n\| < \varepsilon \quad (6)$$

$$\tan \varphi_{k,\text{mob}} = \frac{\tan \varphi_k}{\text{FOS}}, \quad c_{k,\text{mob}} = \frac{c_k}{\text{FOS}}, \quad \tan \psi_{k,\text{mob}} = \frac{\tan \psi_k}{\text{FOS}}, \quad \sigma_{t,\text{mob}} = \frac{\sigma_{t,k}}{\text{FOS}}. \quad (7)$$

Strength reduction method—Partial safety factor concept: FCUT, (γ)

$$R_n = \|f - K(\varphi_{d,\text{mob}}, c_{d,\text{mob}}, \psi_{d,\text{mob}}, \sigma_{t,d,\text{mob}}) \cdot u_n\| < \varepsilon$$

$$\tan \varphi_{d,\text{mob}} = \text{FCUT} \cdot \frac{\tan \varphi_k}{\gamma_\varphi}, \quad c_{d,\text{mob}} = \text{FCUT} \cdot \frac{c_k}{\gamma_c},$$

$$\tan \psi_{d,\text{mob}} = \text{FCUT} \cdot \frac{\tan \psi_k}{\gamma_\psi}, \quad \sigma_{t,d,\text{mob}} = \text{FCUT} \cdot \frac{\sigma_{t,k}}{\gamma_{\sigma,t}} \quad (8)$$

where R represents the strength reduction method; f represents the total force mobilized during shear failure of model stability; K is the matrix of design strength parameters as a function of friction angle, dilatance angle and cohesion; U_n is the displacement obtained during strength failure as a function of design strength parameters and the total force mobilized. ε represents the relative error of the method.

For the analysis of strength reduction method in ULS on Cast3M code, we have used a variable FCUT (FaCtor UTILisation): this factor is the unknown in the stability computation step. In order to use the partial safety concept with Cast3M, one has to reduce the strength parameters with a prescribed partial safety factor to their design value. The model must be stable with this design strength parameters of friction angle and cohesion. The design values of the friction angle and cohesion are multiplied with FCUT and the model is recalculated. As long as there is convergence, the value of FCUT can be reduced. For example, from 1.0 in steps of 0.01 and latter is the accuracy of the solution. If FCUT gets very low, a certain part of the model plastifies and the convergence gets lost, leading to the solution for the factor of utilization. We have using this brute force strategy but if there was an response from PASAPAS or UNPAS in some of its variables on the convergence quality, a more efficient and intelligent servo mechanism could be used for a bracketed search with a lower and upper limit value focusing in to the final solution in few steps. In our brute force algorithm, we have to count down and if the solution of FCUT is 0.32 for example, we need 68 computational runs starting from 1.0 with step size 0.01 with successful convergence, before we arrive at the solution. The failure and shadings are strongly influenced by the value of FCUT. The closer we get to FCUT which makes the solution non-convergent, the clearer the failure curve appears.

4.5. Validation of the elastoplastic calculation program on Cast3M: calculation of bearing capacity and settlement of a strip footing

Before modeling the problem investigated in this paper, we propose to first validate the code written on Cast3M for the elastoplastic calculation of the stability of geotechnical structures.

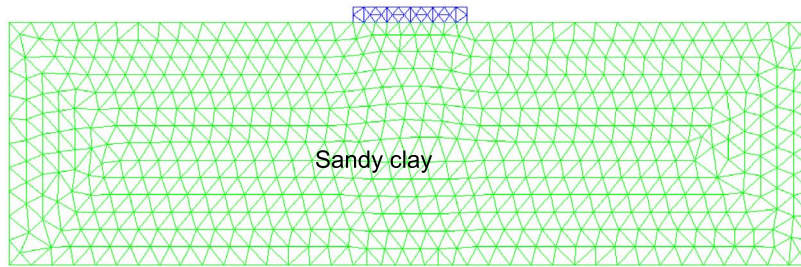


Figure 3. Presentation of the geometry and the view of 2-D mesh of a strip footing.

Table 1. The characteristics of materials for calculation of the footing

| Parameter | Symbol | Sandy clay | Thick concrete | Unit |
|-----------------------------|-------------------------|-----------------|-----------------|-------------------|
| Material model | Model | Mohr–Coulomb | Linear elastic | - |
| Type of behaviour | Type | Drained | Non-porous | - |
| Weight above phreatic level | γ_{unsat} | 16 | 24 | kN/m ³ |
| Weight below phreatic level | γ_{sat} | 18 | - | kN/m ³ |
| Young's modulus | E_{ref} | 5×10^3 | 2×10^7 | kN/m ² |
| Poisson's ratio | ν | 0.35 | 0.15 | - |
| Cohesion | c | 5 | - | kN/m ² |
| Friction angle | φ | 20 | - | ° |
| Dilatancy angle | ψ | 0 | - | ° |

This is the calculation of the bearing capacity of a strip footing whose solution is known. Recall that shortly after isotropic or anisotropic linear elasticity had been introduced into a computer code by the Finite Element Method around 1965, computer scientists proposed algorithms to deal with nonlinear behaviour laws (nonlinear elasticity of Duncan or the perfectly plastic laws) [14, 39, 40]. These laws are developed by rheologists from tests carried out in the laboratory (mainly triaxial and oedometric tests), and they make it possible to better represent the behaviour of soils (appearance of irreversible deformations and rupture).

The plasticity (or failure) criteria are the basis for calculating the limit loads that can be borne by soil masses [35, 41–45]. The Finite Element Method (the unknowns are the displacements and the stresses) makes it possible, by carrying out an incremental calculation, to highlight the value of the limit loads [46–52]. We cite here some contributions to the Finite Element study of foundations on elastoplastic materials in plane strain [16–18, 46–49, 52–61].

Figure 3 shows the view of Cast3M 2-D mesh of a strip footing with $B = 2$ m on a 0.25 m thick concrete on a frictional soil. The thickness of the soil layer is taken 4 m and the material behaviour is represented by Drucker–Prager model for Cast3M [62] calculation and Mohr–Coulomb model for Plaxis calculation (for comparison). The characteristics of material are presented in Table 1. The phreatic level is located in the base of the strip footing.

The Cast3M elasto-plastic calculation is performed in 2-D plane strains. Two calculation phases were carried out, the first phase concerns the simple elastoplastic calculation which makes it possible to obtain the elastoplastic settlement according to the applied load as long as convergence is ensured. The second phase concerns the calculation, the presentation of the shear failure mechanism, the factor of safety as well as the bearing capacity of the strip footing by strength parameters reduction c - ϕ method until failure (non-converging calculation).

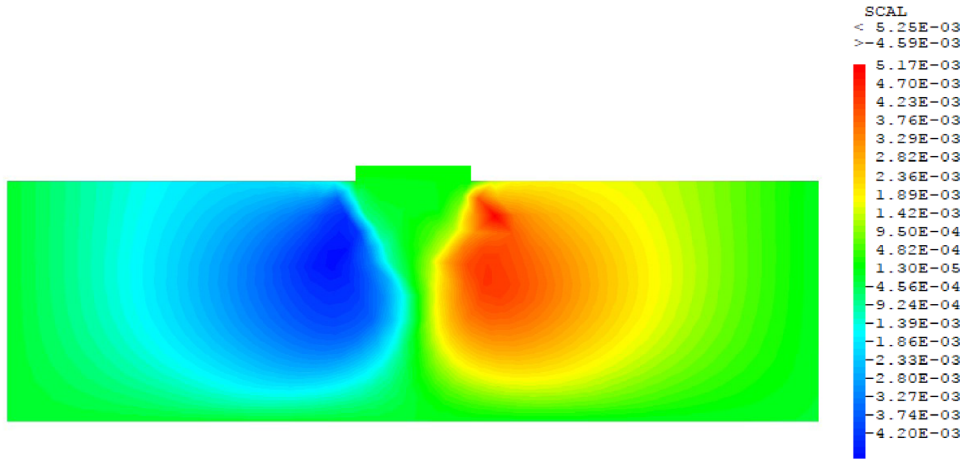


Figure 4. Horizontal displacements (m) at 5th incremental time in SLS of the strip footing submitted at vertical pressure of 100 kPa.

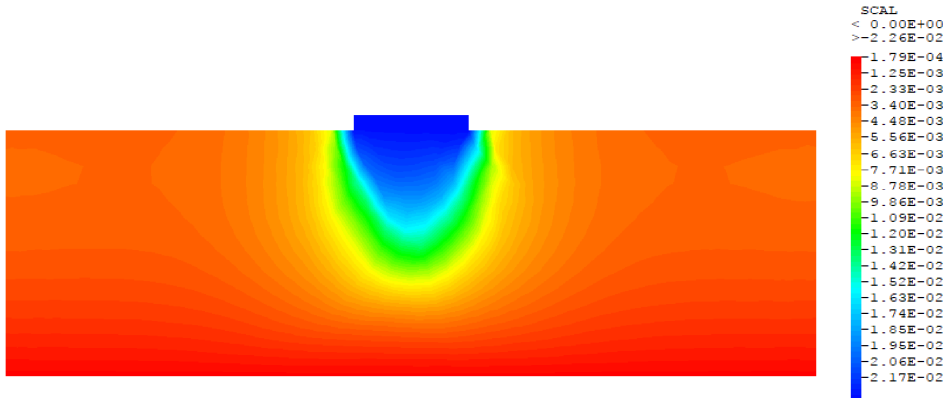


Figure 5. Vertical displacements (m) at 5th incremental time in SLS of the strip footing submitted at vertical pressure of 100 kPa.

Figures 4–9 present the displacements and vertical stresses (in phase 1) of the strip footing submitted at vertical pressure of 100 kPa from elastoplastic analysis. Figure 4 clearly shows the asymmetry of the horizontal displacements in the ground. The vertical displacements isobars are higher under the foundation and gradually decrease until they cancel out as one move away from the point of application of the vertical load (Figures 5 and 6). Figure 7 shows the load displacement curve for the footing at top of thick concrete. The deformed mesh of the model through Figure 8, represents the incremental displacements. The footing sinks following the application of the load causing a heaving of the ground around the footing. The vectors of incremental displacements indeed provide the form of the kinematics failure; this is in agreement with the theoretical results (rigid corner under the foundation (Figure 11)). The total displacement has calculated by the formula: $|U_{total}| = \sqrt{U_x^2 + U_y^2}$.

In the calculation program, each load is applied in 20 increments. For 100 kPa, applied, the pressure corresponding at the 5th increment is 25 kPa (Figures 5–7).

The input value of pressure is 100 kPa and the Factor of Safety reaches approximately 1.0101 (for a calculation carried out with very fine mesh of 1192 elements of the type TRI3 or TRI6).

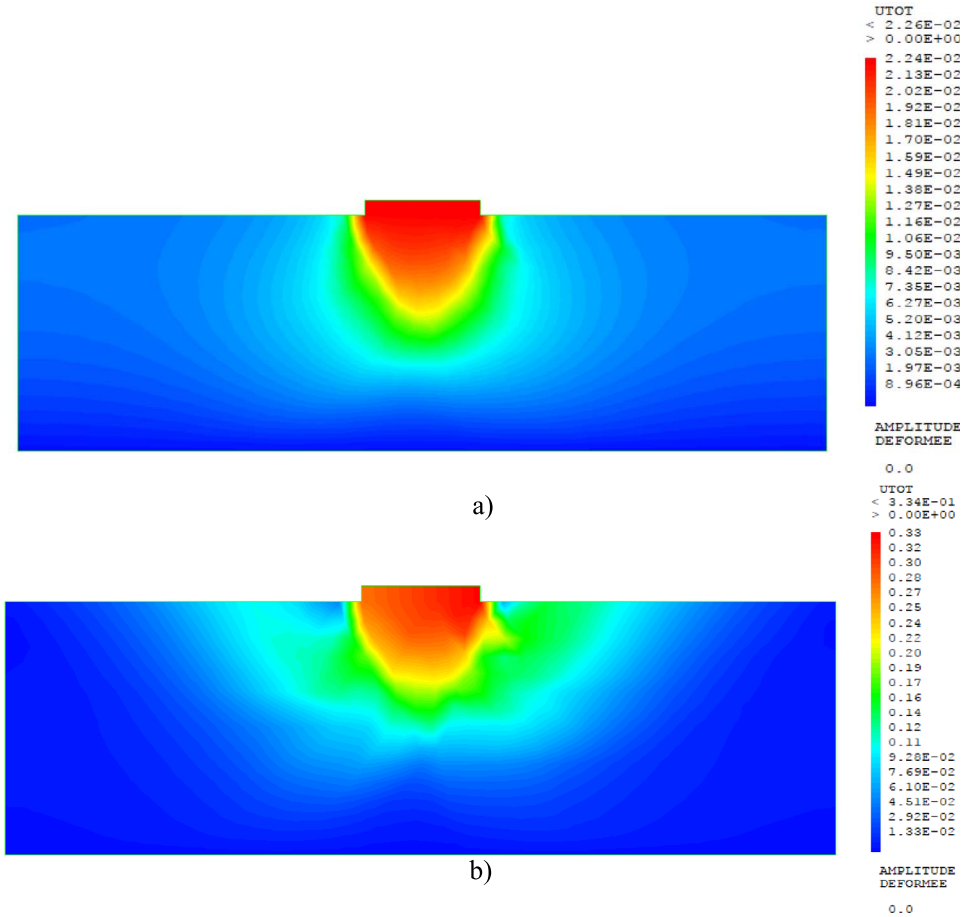


Figure 6. Shadings of total displacements (m) in SLS of the strip footing submitted at vertical pressure of 100 kPa: (a) at 5th incremental time; (b) at full incremental time.

Therefore the failure stress is equal to $100 \text{ kPa} \times 1.0101 = 101.01 \text{ kPa}$. This bearing capacity value should be compared with the reference analytical solutions of Vesic [63], Brinch-Hansen [64, 65], Meyerhof [66, 67] and the solution obtained by the Plaxis software [68]. Given the formula for analytical bearing capacity of a strip footing (Figure 11):

Figure 10 presents the calculation result of phase 2. The shear failure mechanism is clearly represented through the shadings of displacements under the foundation. The calculation stops automatically as soon as the solution is no longer convergent (plastification of the model).

$$\frac{Q_f}{B} = cN_c + \frac{1}{2}\gamma B \cdot N_\gamma \tag{9}$$

$$N_q = e^{\pi \tan \varphi} \cdot \tan^2 \left(45 + \frac{1}{2} \varphi \right) \tag{10}$$

$$N_c = (N_q - 1) \cot \varphi \tag{10}$$

$$N_\gamma = \begin{cases} 2(N_q + 1) \tan \varphi \Rightarrow \text{(Vesic)} \\ 1.5(N_q - 1) \tan \varphi \Rightarrow \text{(Brinch-Hansen)} \\ (N_q - 1) \tan(1.4\varphi) \Rightarrow \text{(Meyerhof)}. \end{cases} \tag{11}$$

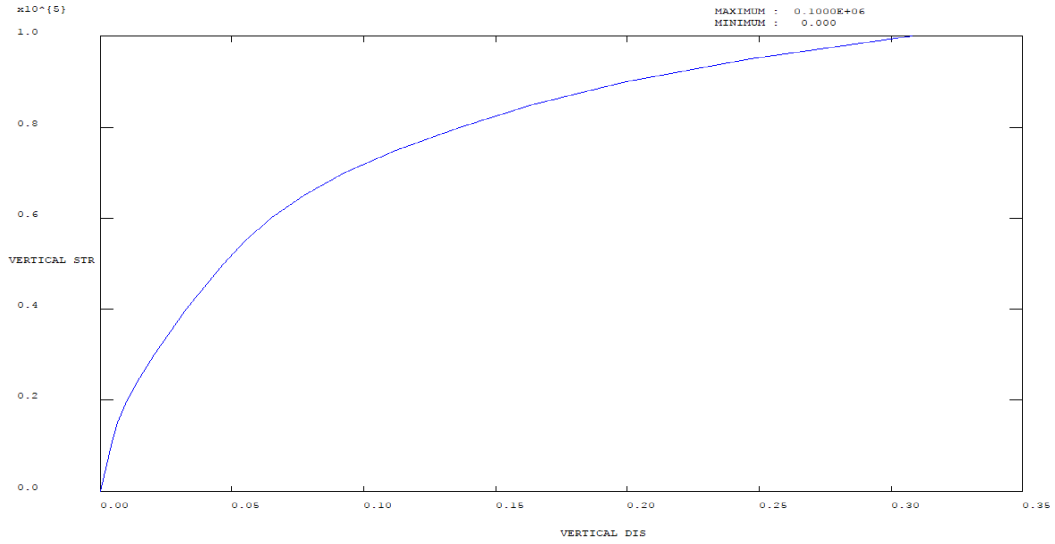


Figure 7. Load displacement curve for the footing.

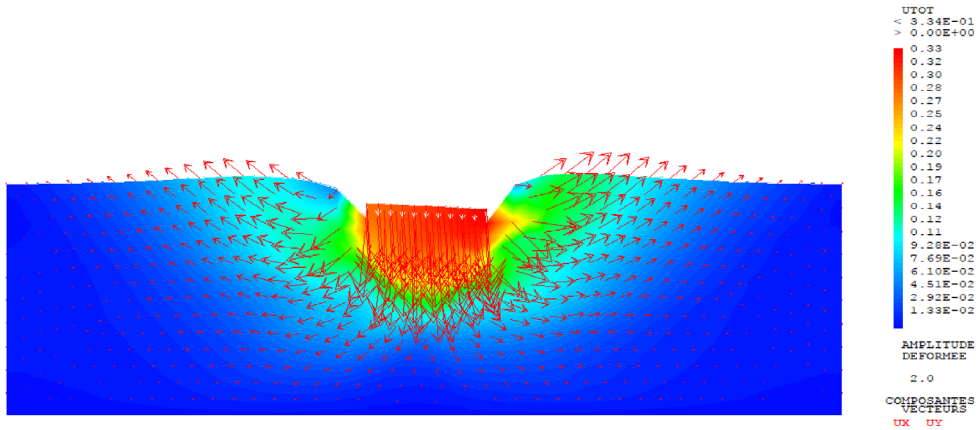


Figure 8. Deformed incremental total displacements (m) at full time in SLS of the strip footing submitted at vertical pressure of 100 kPa (displacements scaled by factor of 2).

Filling in given soil data:

$$N_q = e^{\pi \tan 20} \cdot \tan^2(55) = 6.4$$

$$N_c = (6.4 - 1) \cot(20) = 14.83$$

$$N_\gamma = \begin{cases} 2(6.4 + 1) \tan(20) = 5.39 \Rightarrow \text{(Vesic)} \\ 1.5(6.4 - 1) \tan(20) = 2.95 \Rightarrow \text{(Brinch-Hansen)} \\ (6.4 - 1) \tan(28) = 2.87 \Rightarrow \text{(Meyerhof)}. \end{cases}$$

The effective weight of the soil: $\gamma' = \gamma_{\text{sat}} - \gamma_w = 18 - 10 = 8 \text{ kN/m}^2$

$$\frac{Q_f}{B} = c \cdot N_c + 0.5 \gamma' B \cdot N_\gamma = \begin{cases} 5 * 14.83 + 0.5 * 8 * 2 * 5.39 \approx 117 \text{ kN/m}^2 \Rightarrow \text{(Vesic)} \\ 5 * 14.83 + 0.5 * 8 * 2 * 2.95 \approx 98 \text{ kN/m}^2 \Rightarrow \text{(Brinch-Hansen)} \\ 5 * 14.83 + 0.5 * 8 * 2 * 2.87 \approx 97 \text{ kN/m}^2 \Rightarrow \text{(Meyerhof)}. \end{cases}$$

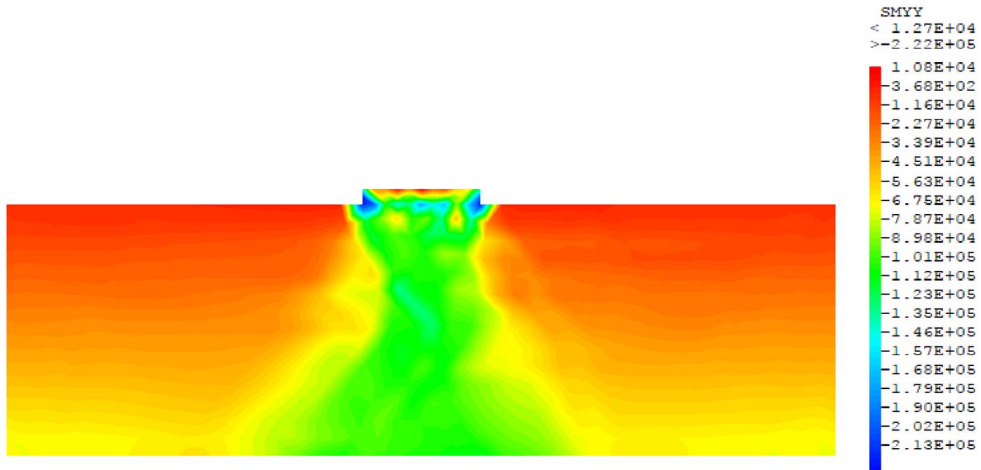


Figure 9. Vertical stresses (Pa) in ULS of the strip footing submitted at vertical pressure of 100 kPa.

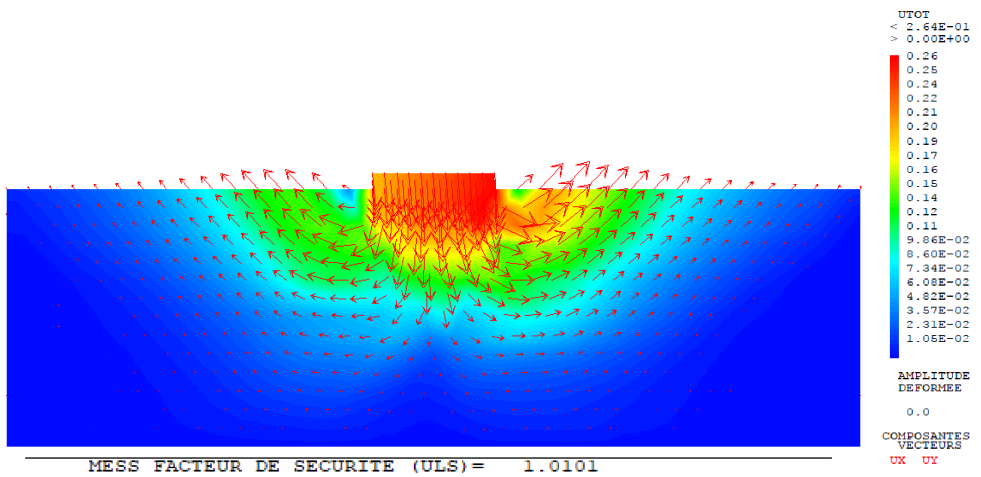


Figure 10. Shadings of shear displacements in ULS (m) and FOS (FOS = 1.0101) of the strip footing submitted at vertical pressure of 100 kPa.

For the results in PLAXIS modeling, in addition to the mesh used in these calculations were performed using a very coarse mesh with a local refinement at the bottom of the footing and a very fine mesh. Fine meshes will normally give more accurate results than coarse meshes. Instead of refining the whole mesh, it is generally better to refine the most important parts of the mesh, in order to reduce computing time. Here we see that the differences are small (when considering 15-noded elements), which means that we are close to the exact solution. The accuracy of the 15-noded element is superior to the 6-noded element, especially for the calculation of failure loads. The results of fine/coarse and 6-noded/15-noded analyses are given below. Table 2 presents the results for the maximum load reached on a strip footing on the drained sub-soil for different 2D and 3D meshes.

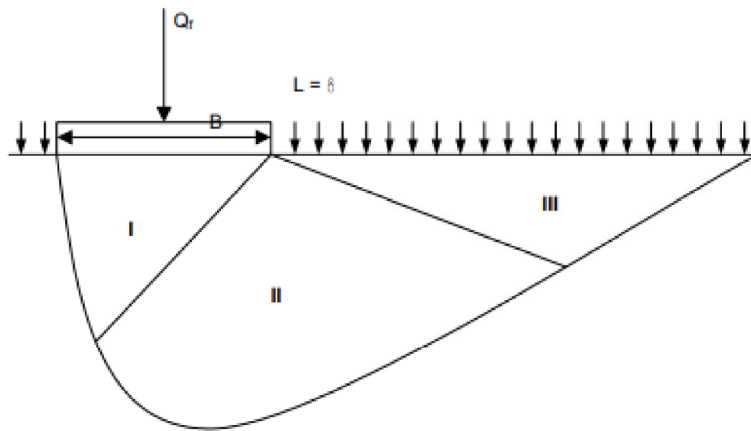


Figure 11. Shear failure mechanism of a shallow foundation for theoretical results.

Table 2. Results for the maximum load reached on a strip footing for 2D (for Cast3M) and different 2D and 3D meshes (for PLAXIS) and analytical solutions

| Solver | Mesh size | Element type | Number of elements | Maximum load (kN/m) | Failure load (kN/m ²) |
|--------------------|---|--------------|--------------------|---------------------|-----------------------------------|
| PLAXIS Code | Very coarse mesh with local refinements under footing | 6-noded | 79 | 281 | 146 |
| | Coarse mesh | 6-noded | 121 | 270 | 141 |
| | Very fine mesh | 6-noded | 1090 | 229 | 121 |
| | Very coarse mesh with local refinements under the footing | 15-noded | 79 | 236 | 124 |
| | Coarse mesh | 15-noded | 121 | 248 | 130 |
| | Very fine mesh | 15-noded | 1090 | 220 | 116 |
| Cast3M code | Very fine mesh | 3-noded | 1192 | - | 101 |
| Analytical results | Vesic | | | | 117 |
| | Brinch-Hansen | | | | 98 |
| | Meyerhof | | | | 97 |

In this Table 2, the failure load for PLAXIS calculation has been calculated as:

$$\frac{Q_f}{B} = \frac{\text{Maximumforce}}{B} + \gamma_{\text{concrete}} * d = \frac{\text{Maximumforce}}{2} + 24 * 0.25. \quad (12)$$

From the above results of PLAXIS, it is clear that fine FE meshes give more accurate results. On the other hand the performance of the 15-noded elements is superior over the performance of the lower order 6-noded elements. Needless to say that computation times are also influenced by the number and type of elements. The Cast3M results are generally in good agreement with the analytical results of the collapse load. The bearing capacity obtained by our elastoplastic modeling on Cast3M is 101 kPa very close to the Brinch-Hansen and Meyerhof reference solutions, validating our calculation program very satisfactorily. For very fine mesh of the numerical model of the footing, the difference between Plaxis and Cast3M results is 7% (Table 2). This gap comes the difference between Drucker-Prager and Mohr-Coulomb materials. Drucker-Prager is the advanced ideal elasto-plasticity model by the number of parameters to determined. He is adequate

Table 3. Results for the maximum load reached on a strip footing for different 2D meshes in Cast3M (partial safety factors: $\gamma_{\sigma t}$) and analytical solutions

| Solver | Mesh size | Element type | Number of elements | Failure load (kN/m ²) | FCUT | $\gamma_{\sigma t}$ | FOS | $\frac{((F_{3\text{-noded}}) - (F_{6\text{-noded}}))}{(F_{6\text{-noded}})} \times 100$ |
|-----------------------|---|--------------|--------------------|-----------------------------------|------|---------------------|-------------|---|
| Cast3M code | Very coarse mesh with local refinements under footing | 3-noded | 76 | 166.66 | 0.65 | 1.08 | 1.67 | 29.93 |
| | Coarse mesh | 3-noded | 120 | 138.89 | 0.65 | 0.90 | 1.39 | 14.59 |
| | Coarse mesh | 3-noded | 242 | 123.46 | 0.65 | 0.80 | 1.23 | 13.89 |
| | Fine mesh | 3-noded | 370 | 111.11 | 0.65 | 0.72 | 1.11 | 6.66 |
| | Very fine mesh | 3-noded | 1192 | 101.11 | 0.65 | 0.66 | 1.01 | 0.00 |
| | Very coarse mesh with local refinements under the footing | 6-noded | 76 | 128.28 | 0.91 | 1.17 | 1.28 | - |
| | Coarse mesh | 6-noded | 120 | 121.21 | 0.91 | 1.10 | 1.21 | |
| | Coarse mesh | 6-noded | 242 | 108.40 | 0.91 | 0.99 | 1.08 | |
| | Fine mesh | 6-noded | 370 | 104.17 | 0.91 | 0.95 | 1.04 | |
| | Very fine mesh | 6-noded | 1192 | 101.10 | 0.91 | 0.92 | 1.01 | |
| Analytical results | Vesic | | | 117 | | | | - |
| | Brinch-Hansen | | | 98 | | | | |
| | Meyerhof | | | 97 | | | | |

to describe the sophisticated and realistic behaviour of geotechnical structure submitted by any load by correcting the shortcomings of Mohr–Coulomb model which only includes five parameters ($E_{\text{ref}}, \nu, c, \phi, \psi$) determined directly from conventional triaxial tests.

The analysis on the mesh density and element type (TRI3 and TRI6) in Cast3M (Table 3) show that, the difference between element type TRI3 and TRI6 results varies between 30 (for the very coarse mesh with local refinements under footing) to 0% (for the very fine mesh). In the developed procedure in this paper, when the mesh is very fine, the adjustment of the factor FCUT (this factor is the unknown in the stability computation step. See part 4.4) makes it possible to regulate numerical gap between the very coarse mesh effect to very fine mesh of the model. Table 3 clearly shows the interest of this factor. For the very fine mesh with TRI3 element, it is reduced progressively by step of 0.01 from 1 to 0.65 (35 steps) to obtain the same result with a TRI6 element whose FCUT is reduced progressively from 1 to 0.91 (9 steps).

The code programming algorithm is made so that at the starting of the calculation a value of FCUT = 1 is introduced. As the calculation evolves, this value is gradually reduced from 1 by steps of 0.01 until a value which allows to have the solution (end of convergence). The global safety factor is therefore obtained automatically at the end of this calculation. It is not necessary to introduce the partial safety factors. After calculation the global safety factor; the partial safety factors are obtained automatically from FCUT adjusted during the calculation and the FOS obtained according to Equation (8). The FOS is not equal to 1/FCUT, because the partial safety coefficients are different from 1. It is also possible to introduce any value n of FCUT less than 1 at the start of the calculation. If this calculation converges, the calculation time which was necessary to reduce FCUT progressively up to n is gained and the calculation continues until the final solution. The values of the partial safety coefficients have been inserted in Table 3.

5. Numerical analysis of retaining walls–slope stability and backfill

The materials used for the backfills come from two different quarries located a few kilometers from the project area. Backfill 1 consists of greyish pozzolan with a strong granular predominance

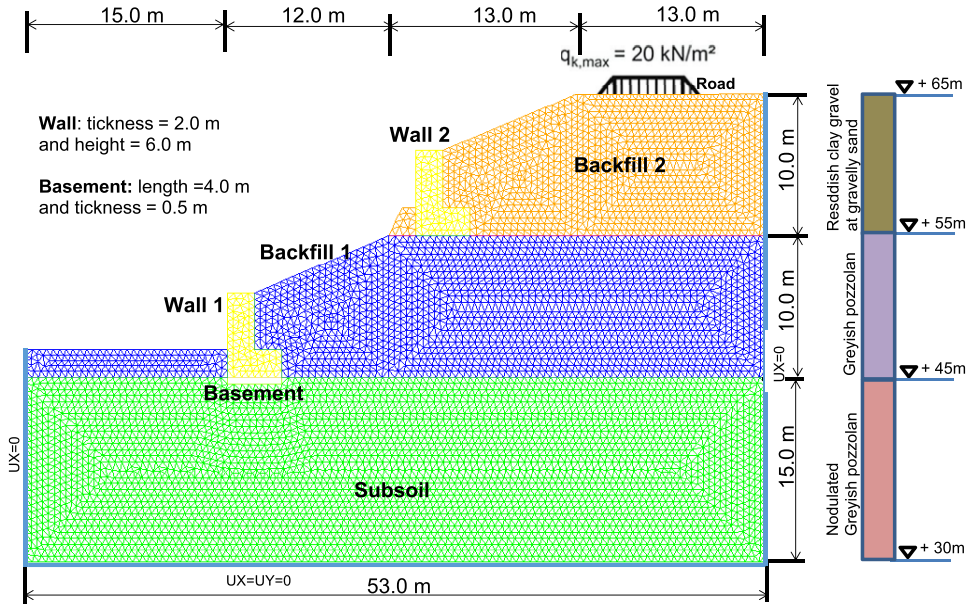


Figure 12. Detailed view of the 2D mesh and soil clusters of retaining walls and backfills.

with a low fines content. Backfill 2 is constituted by the Reddish clay gravel at gravelly sand with a spread out grain size.

The numerical modeling of the retaining structures is made in 2D, plane deformations from the Finite Elements Cast3M calculation code with triangular elements with 3 nodes (TRI3). Figure 12 shows the 2D mesh view of the model and the borehole log with the altimetry of the different backfills and the name of the sedimentary rocks involved. The boundary conditions of the model are standard, i.e. blocking of all displacements at the bottom of the model ($U_x = U_y = 0$) and blocking of horizontal displacements on the left and right bound of the model ($U_x = 0$).

In this paper, our analyze is performed at the Serviceability Limit State (SLS) for deformation-based approach and the Ultimate Limit State analysis (ULS) for stress and strength-based approach. The forces generated by the self-weight of the soil are computed using a standard gravity “turnon” procedure involving integrals over each element of the form:

$$p^{(e)} = \gamma \int_{V^e} N^T d(\text{vol}) \tag{13}$$

where N values are the shape functions of the element and the superscript e refers to the element number. This integral evaluates the area of each element, multiplies by the total unit weight of the soil and distributes the net vertical force consistently to all the nodes. These element forces are assembled into a global gravity force vector that is applied to the FE mesh in order to generate the initial stress state of the problem.

5.1. Materials model

Drucker–Prager model [69], ideal elasto-plasticity without hardening or softening, they constant stiffness parameters are adjusted of strength parameters to the average of Mohr–Coulomb compression and tension. Apart from unit weight gravity γ , Young Modulus E and Poisson’s ratio,

Table 4. Materials properties of the model

| Parameter | Symbol | Subsoil: thick Sandy clay | Basement | Concrete retaining wall 1 & 2 | Backfill 1 | Backfill 2 | Unit |
|--------------------------------|-------------------------|------------------------------|------------------|-------------------------------------|------------------|------------------|-------------------|
| Material model | Model | Mohr–Coulomb | Mohr–Coulomb | Linear elastic | Mohr–Coulomb | Mohr–Coulomb | - |
| Type of behaviour | Type | Drained | Drained | Non-porous | Drained | Drained | - |
| Weight above phreatic level | γ_{unsat} | 20 | 20 | 25 | 20 | 20 | kN/m ³ |
| Young's modulus | E_{ref} | 40×10^3 | 40×10^3 | 4×10^7 | 40×10^3 | 40×10^3 | kN/m ² |
| Poisson's ratio | ν | 0.3 | 0.3 | 0.2 | 0.3 | 0.3 | - |
| Cohesion | c' | 10 | 0.1 | - | 0.1 | 1 | kN/m ² |
| Friction angle | φ' | 20 | 35 | - | 35 | 35 | ° |
| Dilatancy angle | ψ | 0 | 5 | - | 0 | 0 | ° |

this model requires 8 additional parameters, some of which are deduced from the Mohr–Coulomb model for its use in the $F \cdot E$ Cast3M code. Its other parameters are as follows:

$$\text{ALFA} = \text{ETA} = \frac{2\sqrt{3}\sin\varphi}{9 - \sin^2\varphi} \quad (14)$$

$$\text{BETA} = \text{MU} = \text{DELTA} = \sqrt{\frac{2}{3}} \quad (15)$$

$$K = KL = \frac{6\sqrt{3}c \cdot \cos\varphi}{9 - \sin^2\varphi} \quad (16)$$

$$\text{GAMMA} = \frac{2\sqrt{3}\sin\psi}{9 - \sin^2\psi}. \quad (17)$$

In our computations on Cast3M, we have used a variable FCYS (FaCtor Yield Surface) for the built in Drucker–Prager plasticity model. In order to adjust the Mohr–Coulomb strength parameters to the circular cone of the Drucker–Prager failure surface (see Figure 2), different strategies are known. The factor FCYS regulates the adjustment [70]. The value of 0.0 is tension, 1.0 is compression, 0.5 is their average. Other values would mean a weighted result and values above 1.0 use the surface equality approach. Values below 0.0 default to 1.0 and the compression adjustment. In this paper FCYS is fixed at 0.5. Table 4 presents the materials properties of the model. $\text{BETA} = \text{MU} = \text{DELTA} = \sqrt{2/3}$ is implementation specific for Drucker–Prager model in Cast3M.

5.2. Analysis of problem phase by phase: staged construction

To know the contribution of each phase to the global stability, the displacements are calculated at the Serviceability Limit State (SLS) and the Ultimate Limit State analysis (ULS) for stress and strength. The solution strategy is based by treatment of the problem in 2-D plane strain (geometry and mesh), the definition of soils and retaining walls and the definition of all external loads (self-weight and charges) and the implementation of the construction phases by stepwise imposition of loads. The following staged constructions are analyzed in Cast3M: the first phase is based on the application of geostatic stress state in the subsoil and basement (stress adjustment or gravity loading). In phase 2, the retaining wall construction 1 is realized. The layered backfill 1 is realized in phase 3; the retaining wall construction 2 in phase 4; the 2nd layered backfill in phase 5; the application of surface load for road construction following the GTR recommendation [71] (regarded as variable) in phase 6 and the calculation of general stability of the construction in phase 7.

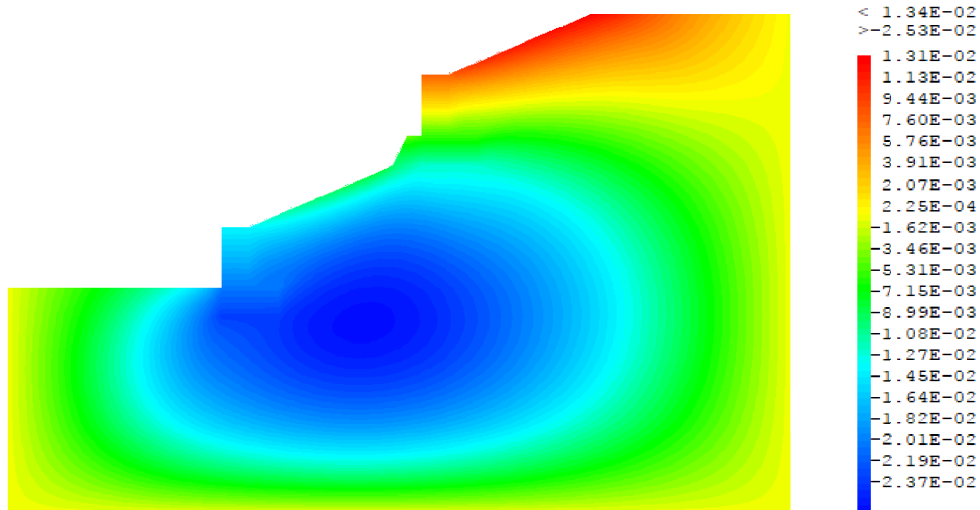


Figure 13. Horizontal displacements: U_x (m) in SLS of the model.

The “turn-on” procedure is described clearly according to the following calculation steps [72, 73]: after generation of the mesh of the global model, the calculation of the elastic phase is carried out in order to obtain the stresses and the elastic displacements in the structure. The elastoplastic calculation is carried out PASAPAS in the code cast3M. Displacements are initialized to zero at the beginning of each phase. Each construction stage of the structure corresponds to a PASAPAS calculation phase in the cast3M code. In each phase, the parameters of the entire model are inserted and the calculation results are logged in a table. The phase number corresponds to the number of calculation tables. The results of each phase are recorded in the tables. From these tables, the next phase begins with the previous phase.

5.3. Phase 0: elastic modeling in one phase

The purpose of the elastic calculation carried out is to obtain the stresses and displacements throughout the model. The entire geotechnical structure is built in a single phase. The gravity load are applied on the model. The objective of this part is to show the limits and insufficiencies of a modeling of a geotechnical structure by using a model with elastic behavior. The results of this part are to be compared with those of part 5.4 whose behavior model realistically describes the behavior of geotechnical structures. Figures 13–16 present the displacements (in phase 0) of the model from elastic analysis.

The interest of the computation of the elastic phase is to obtain displacements and stresses in the model. The total displacement in the elastic calculation phase is 21 cm.

5.4. Drucker–Prager elasto-plastic modeling in staged construction

In this part, the stresses and displacements are calculated for each construction stage up to the Serviceability phase.

5.4.1. Phase 1: elasto-plastic modeling

This phase is based on the application of geostatic stress state in the subsoil and basement (gravity loading). The installation of the subsoil and basement causes the appearance of the

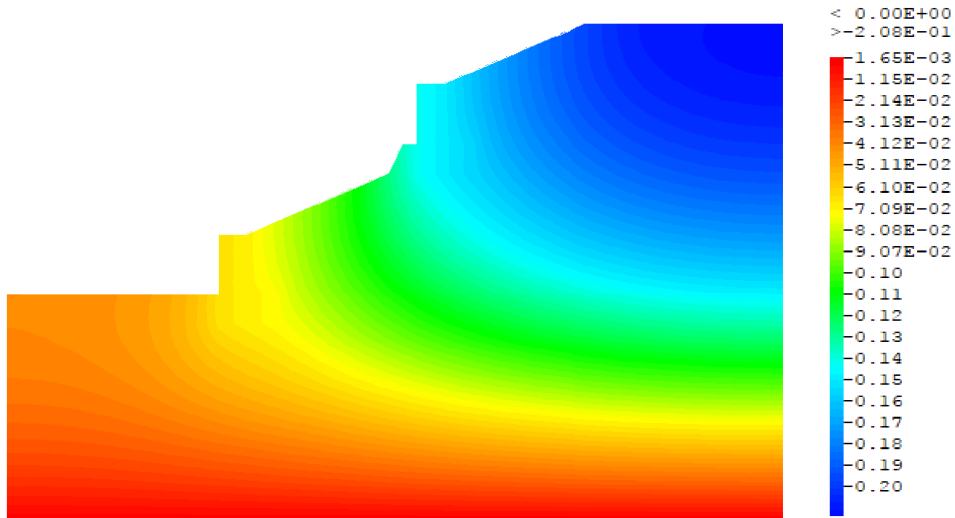


Figure 14. Vertical displacements: U_y (m) in SLS of the model.

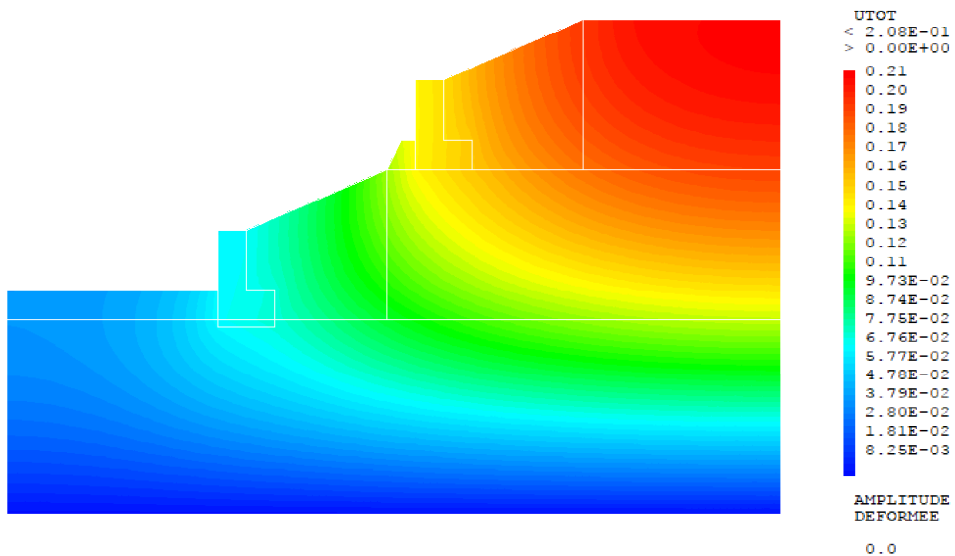


Figure 15. Total displacements (m) in SLS of the model.

vertical, horizontal and total displacements of 3.22 cm due to gravity loading. Figures 17 and 18 present the total displacements and vertical stress (in phase 1) of the model from elastoplastic analysis.

5.4.2. *Phase 2: elasto-plastic modeling*

In this phase 2, the retaining wall 1 is built. This phase begins after phase 1, the displacements are initialized to zero in the model and is based on the application of geostatic stress of the retaining wall 1 on drained sub-soil (gravity loading). Although displacements on the basement and subsoil are controlled with the realization of this one with extra embankment (over-elevation) whose thickness corresponds to the vertical displacement, the construction of

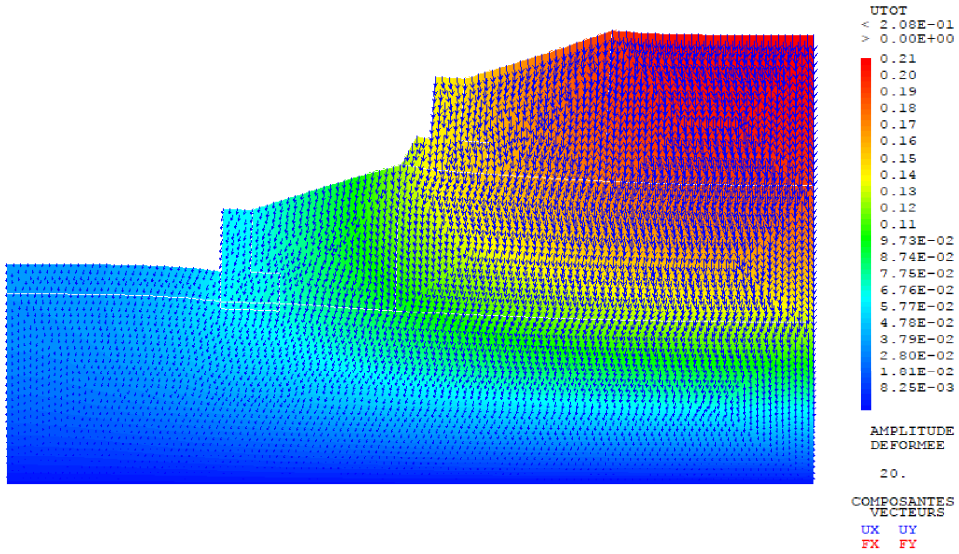


Figure 16. Deformed of the total displacements (m) in SLS of the model (displacements scaled by factor of 20).

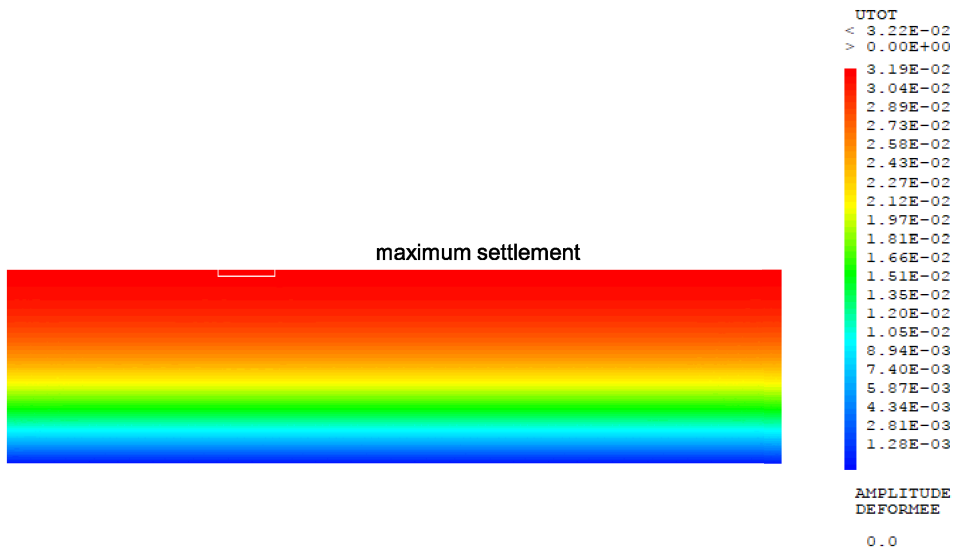


Figure 17. Total displacements (m) in SLS of the subsoil and basement in phase 1.

the retaining wall 1, causes an appearance of settlements of 8.83 cm. Figures 19–21 present the total displacements, vertical plastic strains and vertical stress (in phase 2) of the model from elasto-plastic analysis.

5.4.3. Phase 3: elasto-plastic modeling and the strength reduction method

5.4.3.1. Phase 3.1: elasto-plastic modeling. In this phase 3.1, the layered backfill 1 is realized. This phase starts after phase 2, the displacements are initialized to zero in the model and is based on the application of geostatic stress of the layered backfill 1 on drained sub-soil (gravity loading).

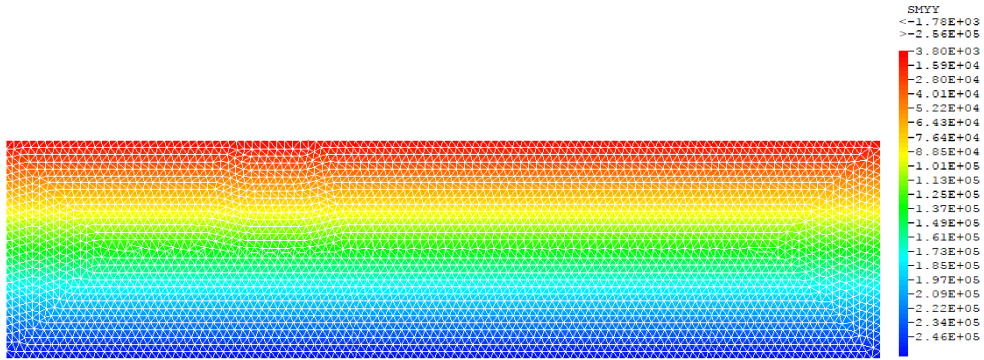


Figure 18. Vertical stress (Pa) of the model in ULS (phase 1).

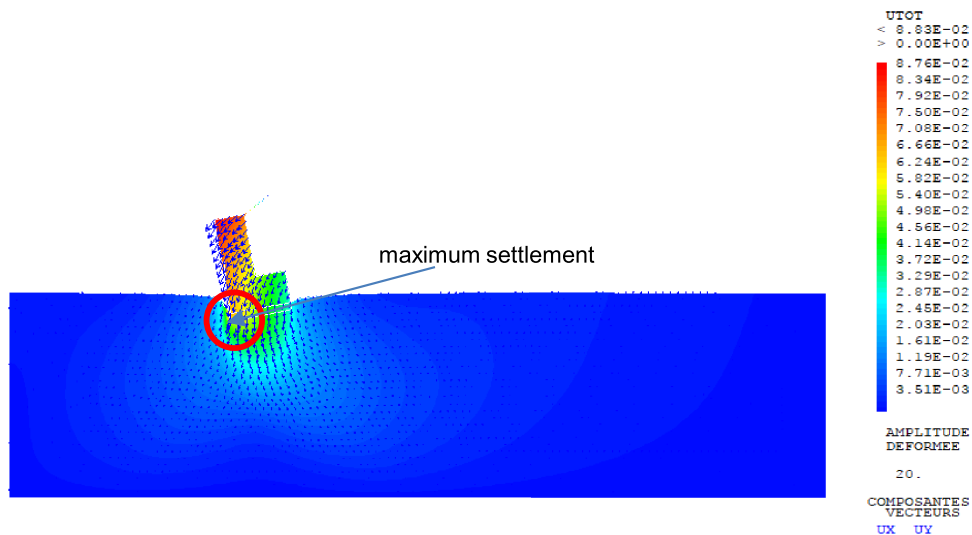


Figure 19. Deformed of the total incremental displacements (m) in SLS of the retaining wall 1 on drained sub-soil (displacements scaled by factor of 20) in phase 2.

Figures 22–24 present the total displacements, plastic strains and vertical stress (in phase 3.1) of the model from elastoplastic analysis. Although the displacements are reset to zero on the subsoil, basement and on the retaining wall 1, the construction of layered backfill 1 generates a horizontal displacement of the wall and the total displacements of 15 cm due to its own weight.

5.4.3.2. Phase 3.2: strength reduction method. This phase starts after phase 3.1, the displacements are initialized to zero in the model. The analysis is based on the limit equilibrium of external and internal forces in the model (gradual reduction of the mobilized strength). In the Cast3M calculation code, the advanced solution is performed on recursive reduction of the mobilized strength using a search strategy based on a convergence criterion. The part 4.4 describe the concept of the strength reduction method developed in this paper. Phi-c reduction phase cannot be used as a starting condition for another calculation phase because it ends in a state of failure. Therefore it is advised to define all safety analyses at the end of the list of calculation phase and to use the start from phase parameter as a reference to the calculation phase for which a safety factor is calculated.

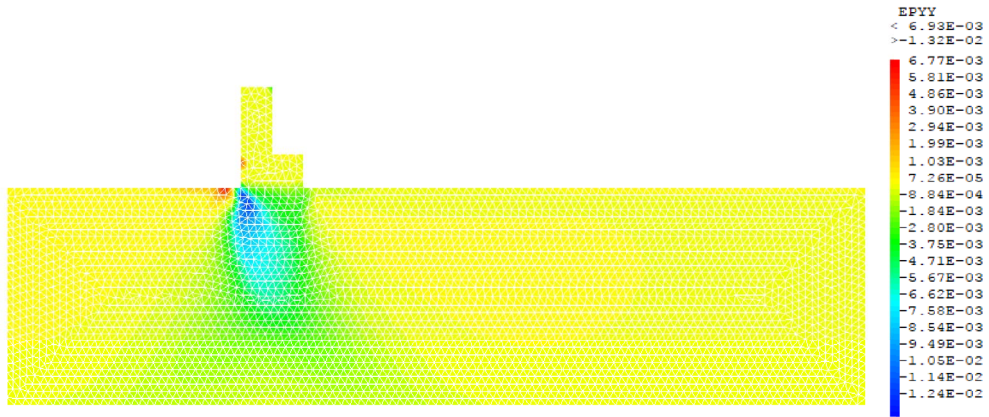


Figure 20. Vertical plastic strains in SLS of the retaining wall 1 on drained sub-soil in phase 2.

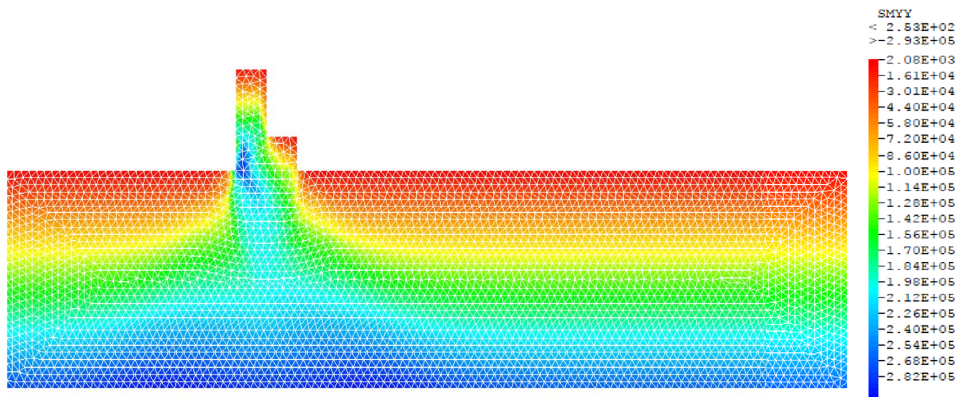


Figure 21. Vertical stress (Pa) of the model in ULS (phase 2).

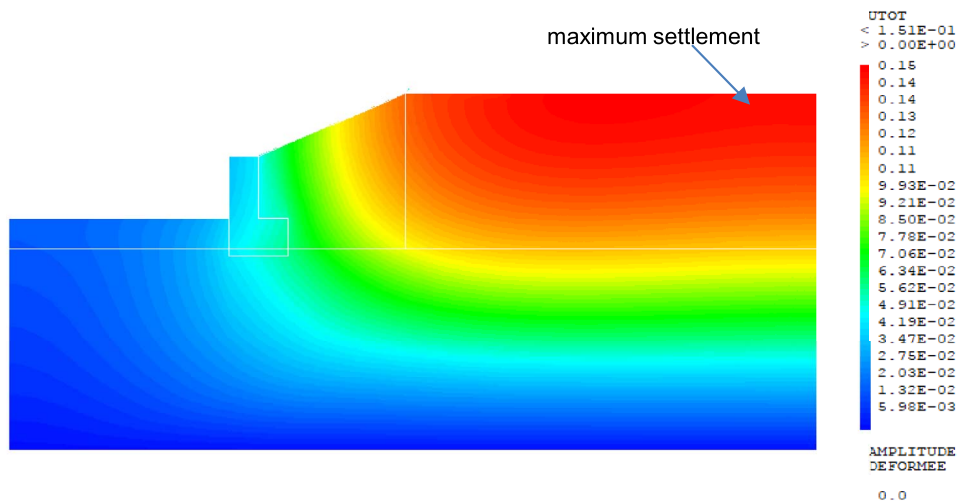


Figure 22. Total displacements (m) in SLS of the model in phase 3.1.

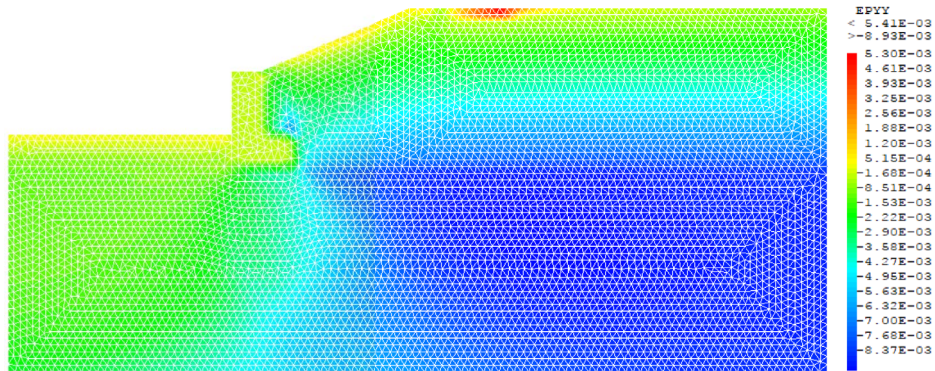


Figure 23. Vertical plastic strains in SLS in phase 3.1.

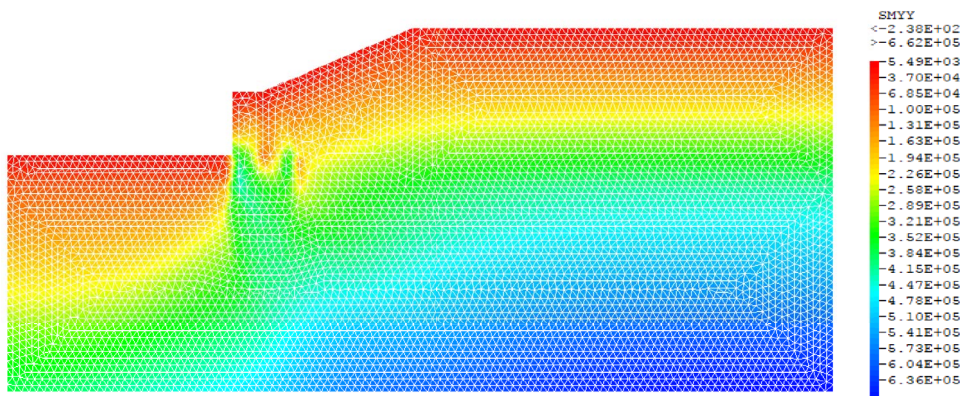


Figure 24. Vertical stress (Pa) of the model in ULS (phase 3.1).

The Factor of Safety calculation procedure is based on the calculation of a stable initial stress and corresponding deformation state recursive reduction of the shear and tensile strength until a convergence to a prescribed tolerance is still obtainable. The restrictions on suitable material behaviour of Drucker–Prager, which is the ideal elasto-plasticity are considered. This model is adequate to describe the sophisticated and realistic behaviour of geotechnical structure submitted by any load. Figure 25 presents the total shear displacements (in phase 3.2) of the model from c-phi reduction strength method (ULS, GEO-3). In this phase the Factor of Safety is $FOS = 1.5625$. The duration of the calculation in this phase is 40 min.

The benefit of this intermediate calculation phase is to verify the stability of the structure after the installation of the thick backfill before continuing with the other construction phases. According to the result of this phase, the sliding FOS is equal to 1.56 guaranteeing the stability of the structure despite the shear displacements of 71 cm which are canceled by the extra embankment and the abutment of the retaining wall 1. In order to validate our elastoplastic calculation program for the c-phi parameters reduction on Cast3M, the results of this part were compared with those of other geotechnical software commonly used in industrial environments. For these modeling with these other softwares, the behaviour of materials obeys the criterion of rupture of Mohr–Coulomb. Several software or methods were used for the comparison of the results.

These include: ULS-Geo-3, failure kinematics with the code Flac2D (FDM); ULS-Geo-3, failure kinematics with the code Tochnog (FEM); LEM, Limit Equilibrium Method; KEM, Kinematic

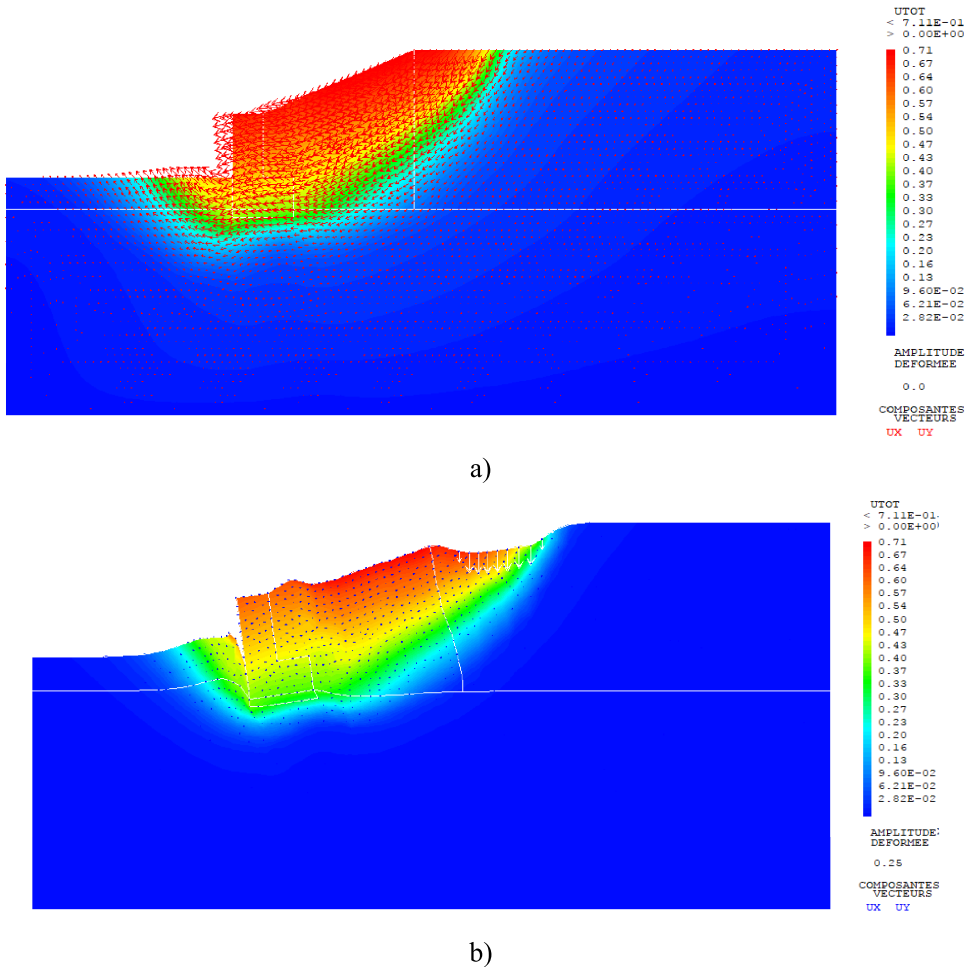


Figure 25. (a) Shadings of shear total incremental displacements (m); (b) shadings of deformed of the total shear incremental displacements (m) in ULS of the model (displacements scaled by factor of 0.25) in phase 3.2.

Element Method; Method of slices with circular slip surface (Bishop method); Method of slices with polygonal slip surface (Janbu method) and Strength Reduction Finite Element Limit Analysis (SR-FELA) [33] implemented in OPTUM G2 [74]. The results in Figure 26 show the shear failure mechanisms of the structure. The comparative FOS values obtained for each method [9, 62, 68, 74–77] are summarized in Table 5. The FOS obtained in our calculation is 1.56. It is the same value that is obtained for the other Finite Element calculation codes presented (TOCHNOG and PLAXIS) in Table 5. This calculation phase 3.2 is very useful, because it makes it possible to know whether the structure is stable before to continue construction. With this FOS = 1.56, the safety of this part of the structure is guaranteed.

The limit equilibrium methods for assessing the stability of earth structures are now used routinely in practice. In spite of this extensive use, the fundamentals of the methods are often not that well understood and expectations exceed what the methods can provide. The fact and implications that limit equilibrium formulations are based on nothing more than equations of statics with a single, constant factor of safety is often not recognized. A full appreciation of the

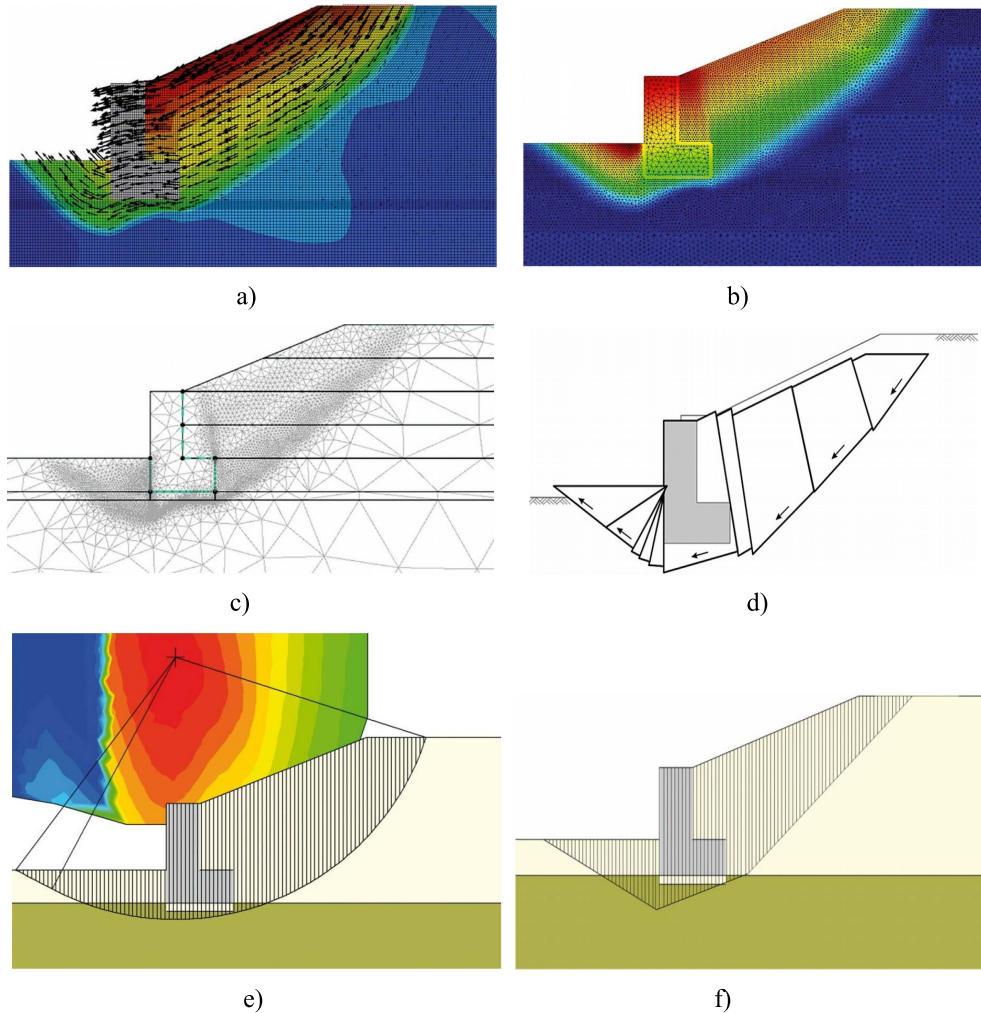


Figure 26. (a) Total displacements in Ultimate Limit State with the code Flac3D (FDM); (b) total displacements in ULS with the code Tochnog (FEM); (c) ULS analysis with the Limit Equilibrium Method (LEM); (d) ULS analysis with the Kinematic Element Method (KEM); (e) ULS analysis with the method of slices (Bishop method); (f) ULS analysis with the method of slices (e.g, Janbu method).

implications reveals that the method has serious limitations. The main limitation is the need to guess the general form of the failure surface in advance, with poor choices giving poor estimates of the failure load. In practice, the correct form of the failure surface is often not intuitively obvious, especially for problems with an irregular geometry, complex loading, or complicated stratigraphy [32, 33]. There are other shortcomings of the technique, as follows.

- (a) The resulting stresses do not satisfy equilibrium at every point in the domain.
- (b) There is no simple means of checking the accuracy of the solution.
- (c) It is hard to incorporate anisotropy, discontinuity and inhomogeneity.
- (d) The analysis does not take into account the dilatancy of the materials and does not directly obtain the stresses and displacements in the structure.

Table 5. The comparison the results of different method [9, 62, 68, 74–77]

| Solver | Method | FOS | Deviation (%) |
|----------------------|---------|---|---------------------|
| OPTUM G2 (2022) | SR-FELA | 1.5–1.6 (lower and upper bound) 1.55 ± 0.032 (exact solution) | –3.22 to +3.22 - |
| PLAXIS (2018) | FEM | 1.56 | +0.65 |
| TOCHNOG (2022) | FEM | 1.56 | +0.65 |
| FLAC (2019) | FDM | 1.63 | +5.16 |
| KEM | KEM | 1.58 | +1.94 |
| Bishop (Talren 2020) | Slices | 1.89 | +21.94 |
| Janbu | Slices | 1.44 | –7.10 |
| Cast3M | FEM | 1.56 | +0.65 |

- (e) The failing soil mass is divided into slices for the calculation. The accuracy of the result depends on the width of each slice. A thin slice width allows to have a valid result.
- (f) It is difficult to generalise the procedure from two to three dimensions.
- (g) It is now possible to deal highly irregular porewater pressure conditions, a variety of linear and nonlinear shear strength models, virtually any kind of slip surface shape, concentrated loads, and structural reinforcement.

However, owing to the inherent assumptions of limit equilibrium analyses, this method does not always furnish a unique factor of safety and it is therefore unsuitable for generating a reference solution for assessing the accuracy of alternative methods. To use limit equilibrium methods effectively, it is important to understand and comprehend the inherent limitations. The c-phi reduction method has been used in Plaxis and Tochnog software. c-phi reduction is an option available in Plaxis [68] to compute safety factors. In the phi-c reduction approach the strength parameters $\tan \varphi$ and c of the soil are successively reduced until failure of the structure occurs. The total multiplier ΣMsf is used to define the value of the soil strength parameters at a given stage in the analysis:

$$\Sigma Msf = \tan(\varphi'_{\text{input}}) / \tan(\varphi'_{\text{reduced}}) = c'_{\text{input}} / c'_{\text{reduced}} \quad (18)$$

$$SF = \text{available strength} / \text{strength at failure} = \text{value of } \Sigma Msf \text{ at failure.} \quad (19)$$

A feature to OptumG2 [74] is the ability to compute rigorous upper and lower bounds on the factor of safety. This allows the user to bracket the exact solution from above and below. More precisely, if we denote the exact solution by E and the lower and upper bounds by L and U respectively, the following inequalities hold: $L \leq E \leq U$. Moreover, if we denote the mean value of the upper and lower bounds by $M = (L + U)/2$, we may define an absolute error by $\varepsilon_{\text{abs}} = (M - L) = (U - M)$.

So that the exact solution may be expressed as:

$$E = M \pm \varepsilon_{\text{abs}} [\%]. \quad (20)$$

The comparison of Cast3M result with different methods commonly used in geotechnics and exact solution (gap: 0.65%) shows that the implementation of c-phi reduction method is successful.

5.4.4. Phase 4: elasto-plastic modeling

In this phase 4, the retaining wall 2 is built on first layered backfill. This phase starts after phase 3.1, the displacements are initialized to zero in the model and is based on the application of geostatic stress (gravity loading) and the stresses add up from one phase to the following.

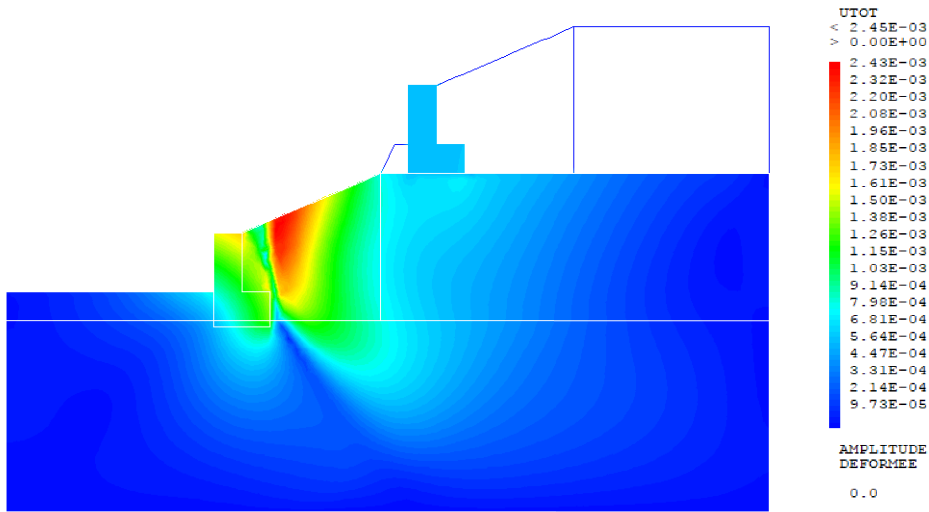


Figure 27. Total displacements (m) in SLS of the model in phase 4.

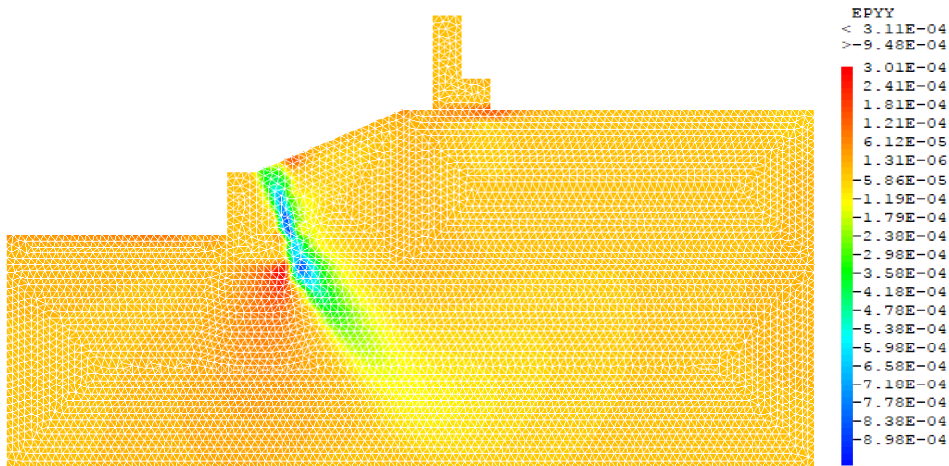


Figure 28. Vertical plastic strains in SLS in phase 4.

Figures 27–29 present the total displacements, vertical plastic strains and vertical stress (in phase 4) of the model from elastoplastic analysis. The construction of the retaining wall 2 above the first layered backfill generates minor settlements on it without prejudice to the stability of the structure.

5.4.5. *Phase 5: elasto-plastic modeling*

In this phase 5, the 2nd layered backfill is realized on first layered backfill. This phase starts after phase 4, the displacements are initialized to zero in the model and is based on the application of geostatic stress (gravity loading). Figures 30 and 31 present the total displacements and vertical stress (in phase 5) of the model from elastoplastic analysis. The construction of the layered backfill 2 above the first layered backfill, generates a negligible horizontal displacement of the wall 2 and minor settlements on the latter without prejudice to the stability of the structure.

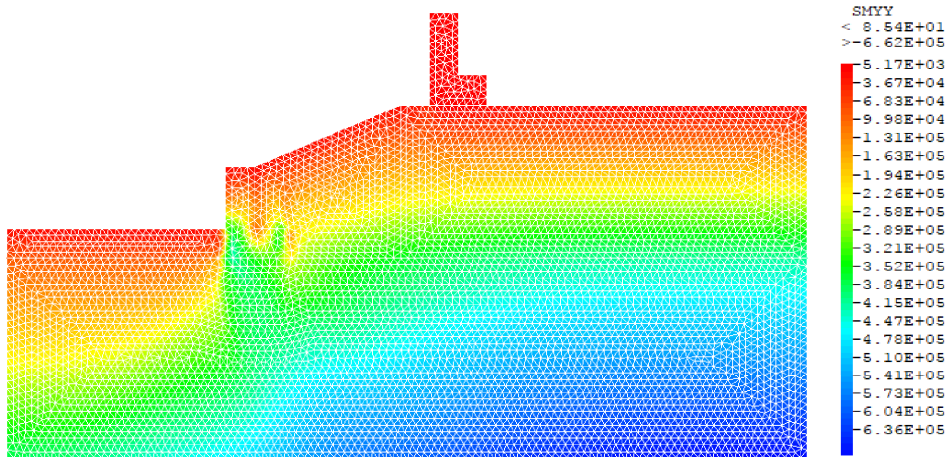


Figure 29. Shadings of the vertical stress (Pa) of the model in ULS (phase 4).

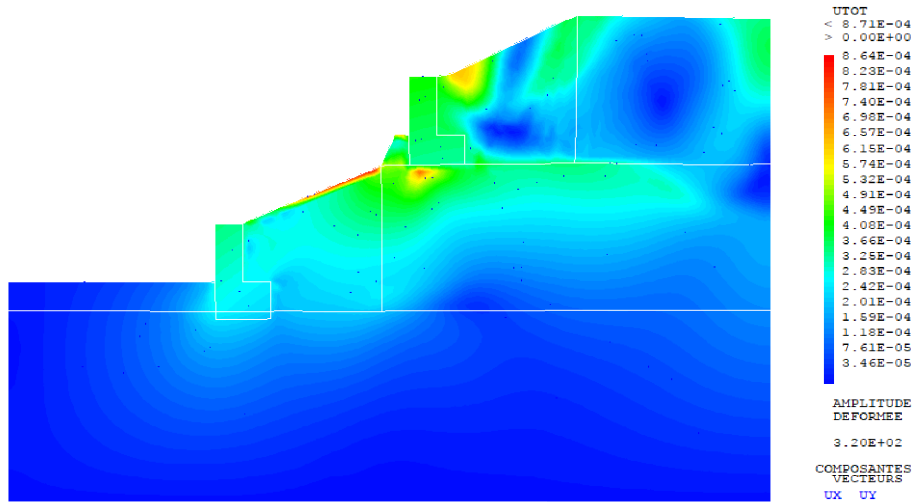


Figure 30. Deformed of the total incremental displacements (m) in SLS of the model (displacements scaled by factor of 320.0) in phase 5.

The thrust of the wall is controlled by the construction of an additional stop corresponding to the projected horizontal displacement due to the thrust of the retaining wall 2.

5.4.6. Phase 6: elasto-plastic modeling

In this phase 6, the application of surface load for road construction following the GTR recommendation [71] (20 kN/m^2 , regarded as variable in Figure 12) is realized on 2rd layered backfill. This phase starts after phase 5, the displacements are initialized to zero in the model and is based on the application of surface load and the stresses add up from one phase to the following. Figures 32–35 present the total displacements, plastic strains and vertical stress (in phase 6) of the model from elastoplastic analysis. The total displacements obtained are small (0.56 cm), these are quickly canceled by the creation of extra embankment whose thickness is equal to the provisional displacement of this phase.

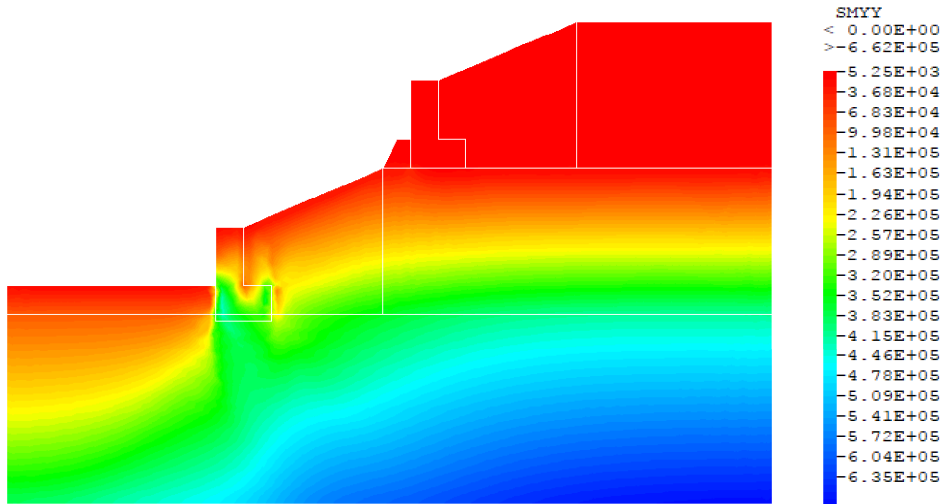


Figure 31. Shadings of the vertical stress (Pa) of the model in ULS (phase 5).

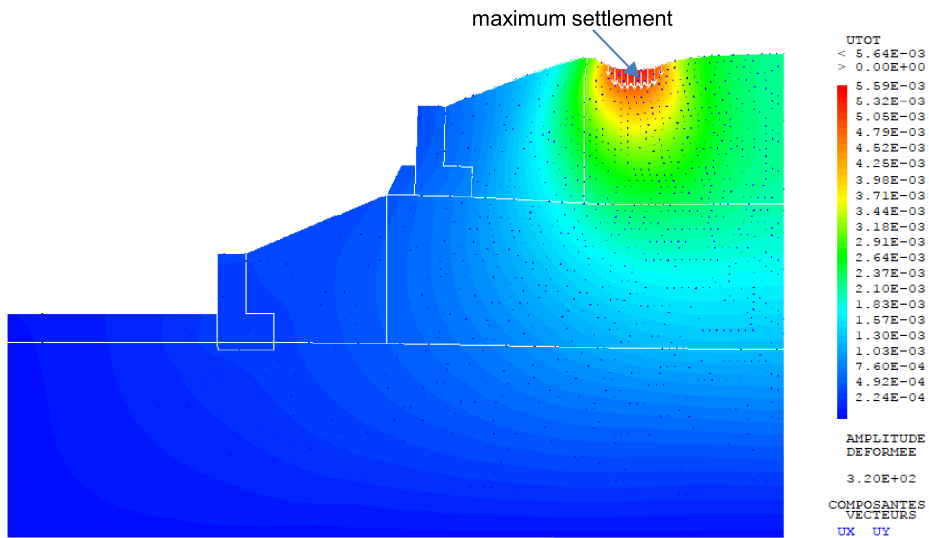


Figure 32. Shadings of the deformed of the total incremental displacements (m) in SLS of the model (displacements scaled by factor of 320.0) in phase 6.

5.4.7. Phase 7: elasto-plastic modeling and strength reduction method

5.4.7.1. Phase 7.1: elasto-plastic modeling. In this phase 7.1, the entire geotechnical structure is built in a single phase, there are no previous phases. The gravity load and surface load are applied on the model. Figure 36 presents the total displacements (in phase 7.1) of the model from elastoplastic analysis. The total displacement in a single phase is 49 cm. This calculation is complementary in order to have the difference in term of displacements if the structure were built in one phase. Which does not represent the practical reality. On the other hand, it is to be compared with that of phase 0 (part 5.3), carried out in linear elastic behavior.

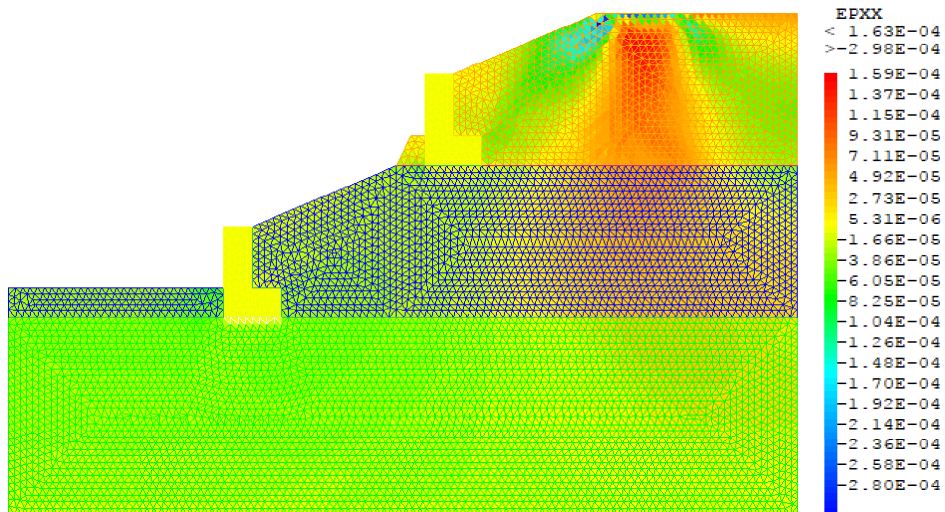


Figure 33. Horizontal plastic strains in SLS in phase 6.

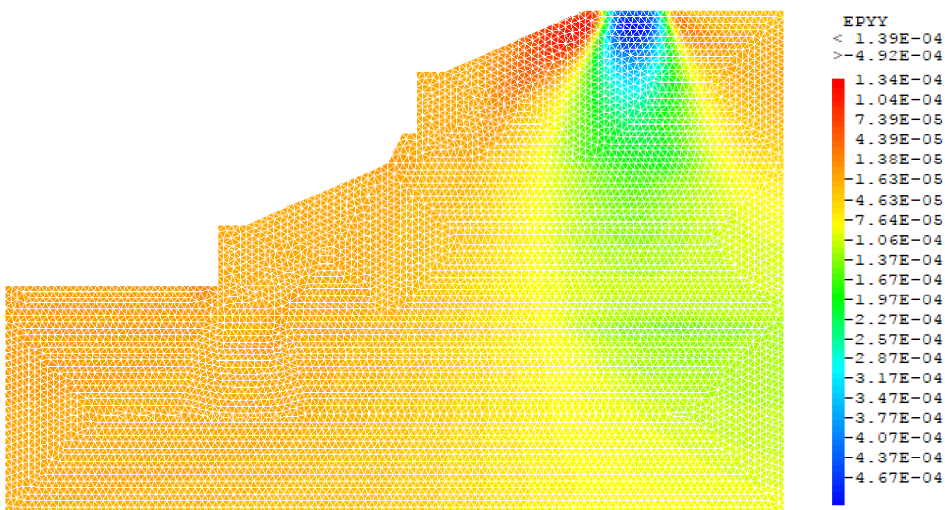


Figure 34. Vertical plastic strains in SLS in phase 6.

5.4.7.2. Phase 7.2: strength reduction method. In this phase 7.2, the gravity load and surface load are applied on the model. This phase starts from phase 7.1. Figures 37 and 38 present the horizontal displacements (in phase 7.2) and the shadings of shear total incremental displacements of the model from c-phi strength reduction method (ULS, GEO-3) analysis and displayed adequate failure kinematics. The factor of safety for this phase is equal to 1.72 guaranteeing the stability of the geotechnical structure despite the shear displacements of 73 cm.

In this phase, Plaxis software has been used (using Mohr-Coulomb model for soils) for the comparison of the results (Figure 39). The factor of safety for this phase obtained by Plaxis software is equal to 1.61. The Cast3M results are generally in good agreement with the Plaxis results of the factor of safety. The difference between the two safety factor values is 6.83%.

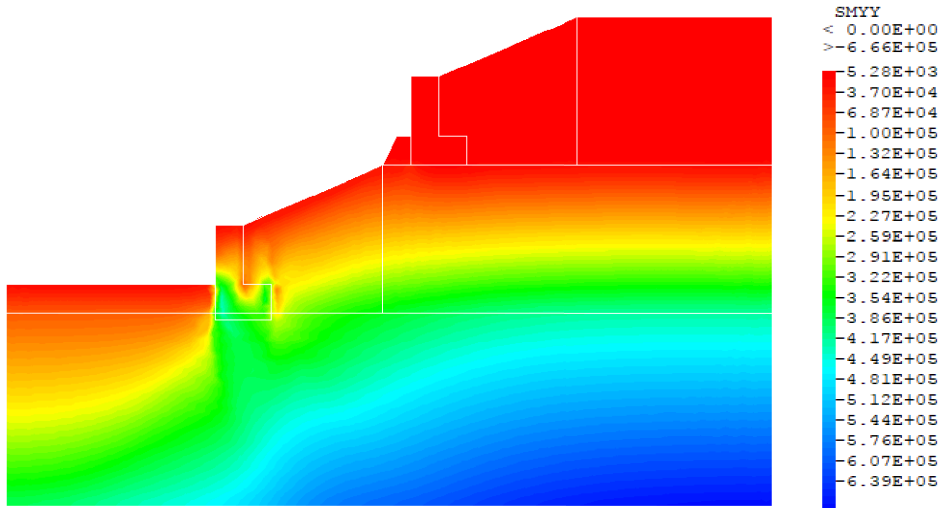


Figure 35. Shadings of the vertical stress (Pa) of the model in ULS (phase 6).

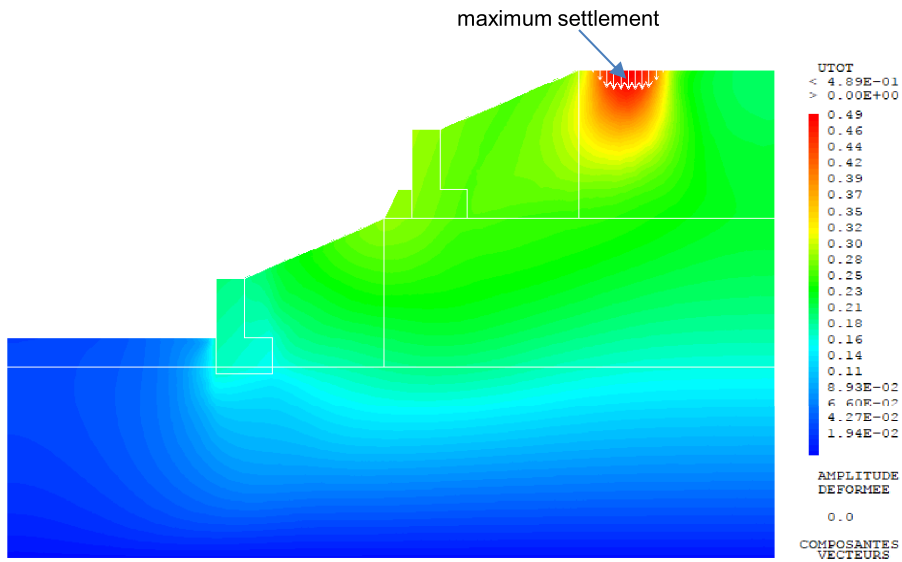


Figure 36. Shadings of the total displacements (m) in SLS of the model in phase 7.1.

This gap can be justified by the fact that the very fine mesh of Plaxis only has 818 elements at 15-noded (not possible to refine beyond) whereas the global model of Cast3M has 1800 elements TRI3.

Table 6 presents the results of the displacements and the Factor of Safety on the model phase by phase. The displacements of the elasto-plastic calculation are higher compared to the elastic calculation (Table 6). In this paper, our computations were carried out respecting the practical phasing of construction of the geotechnical structures. The advantage of staged construction is to know the displacements generated after the construction of each phase. This technique makes it possible to build each phase by providing on the one hand the extra embankment whose

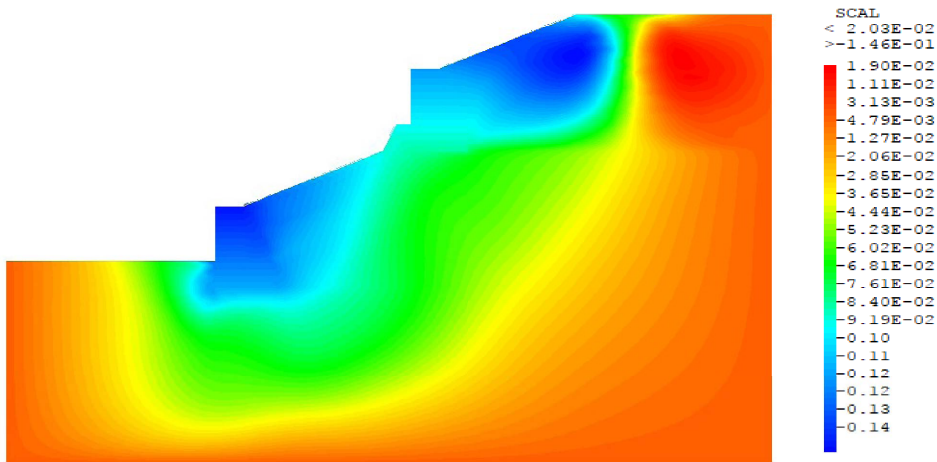


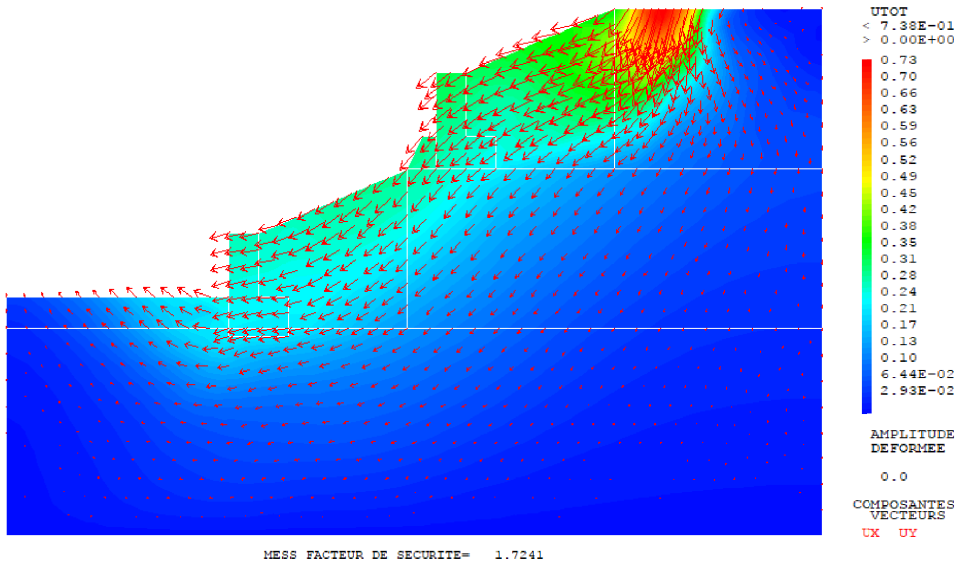
Figure 37. Shadings of horizontal displacements (m) in ULS of the model in phase 7.2.

Table 6. Summary of the results of the displacements by phase

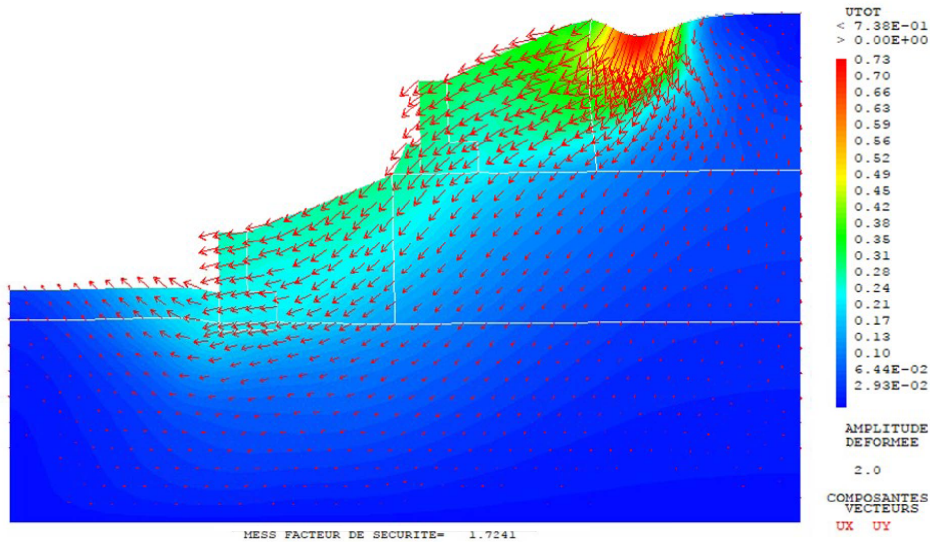
| Calculation phase | Description of phase | Calculation type | Total displacement (cm) | Factor of safety |
|-------------------|--|------------------|-------------------------|------------------|
| Phase 0 | Initialization of initial stresses | Linear elastic | 21 | - |
| Phase 1 | Application of geostatic stress in the Subsoil and basement | Elasto-plastic | 3.22 | - |
| Phase 2 | Application of geostatic stress of the retaining wall 1 | Elasto-plastic | 8.83 | - |
| Phase 3.1 | Application of geostatic stress of the layered backfill 1 | Elasto-plastic | 15 | - |
| Phase 3.2 | Gradual reduction of the mobilized strength | c-phi reduction | 71 | 1.56 |
| Phase 4 | Application of geostatic stress of the retaining wall 2 | Elasto-plastic | 0.24 | - |
| Phase 5 | Application of geostatic stress of layered backfill 2 | Elasto-plastic | 0.087 | - |
| Phase 6 | Application of the surface load | Elasto-plastic | 0.56 | - |
| Phase 7.1 | The gravity load and surface load are applied on the model in single phase | Elasto-plastic | 49 | - |
| Phase 7.2. | Gradual reduction of the mobilized strength on the model | c-phi reduction | 73 | 1.72 |

extra elevation corresponds to the provisional settlements of this phase and on the other hand an additional buttress if necessary so the thickness corresponds to the provisional horizontal displacement caused on the retaining wall.

After construction of the phase, the displacements are obtained and the structure returns to its initial position of stability provided during the design. From this staged construction modeling, it becomes easy to control and limit settlement according to the functional requirements of the geotechnical structure.



a)



b)

Figure 38. (a) Shadings of shear total incremental displacements (m); (b) shadings of deformed of the total shear incremental displacements (m) in ULS of the model (displacements scaled by factor of 2) in phase 7.2.

The safety factor obtained after the construction of the entire geotechnical structure (phase 7) is 1.72, therefore higher than the 1.56 obtained after the construction of backfill 1 (phase 3.2). This increase is due to the fact that, backfill 2 has a cohesion value 10 times greater than that used on backfill 1. These materials come from two different quarries. Backfill 1 consists of materials with a strong granular predominance (greyish pozzolan) with a low fines content. Backfill 2 is constituted by the materials with a spread out grain size (Reddish clay gravel at gravelly sand).

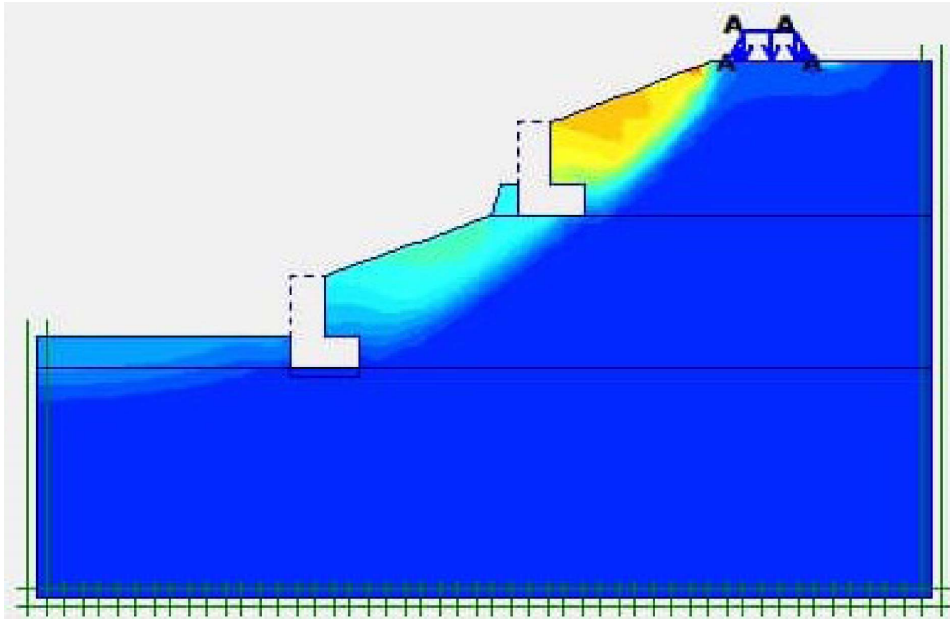


Figure 39. Shadings of shear total incremental displacements (m) calculated by Plaxis.

6. Discussion

The implementation of a c - ϕ reduction procedure in Cast3M shows that this approach, which is often used as a black box in geotechnical softwares, can be implemented in rigorous way. This procedure is first validated on a simple example of bearing capacity of a strip footing and then used to evaluate the stability factor of a geotechnical structure composed of two levels of backfill retained by two retaining walls, with a road built on the top of the second backfill.

6.1. Footing results

Concerning the modeling results of the strip footing, the difference in the theoretical results obtained (formulas (9) and (11)) is in agreement with the assumptions made for each method for the parameter $N\gamma$. The “exact” theoretical expression of $N\gamma$ is not known. Only the upper and lower bounds have been determined in particular by Vesic [63], Brinch-Hansen [64, 65] and Meyerhof [66, 67]. Brinch-Hansen [64–66] indicates its value of $N\gamma$ is a lower bound and that the addition of the three bearing capacity terms, which does not correspond exactly to the real failure mechanism, corresponds to an underestimation of the bearing capacity which is generally less than 20%. It is also this lower bound modified, which is used in Meyerhof’s formula. For the Vesic formula, the upper bound of $N\gamma$ is used. It indicates that the addition of the three bearing capacity terms gives an approximative estimate with less than 10% error over the interval $15 < \phi < 45^\circ$.

The bearing capacity value of 101 kPa obtained by Cast3M modelling with a very fine mesh is regarded as the exact solution because included between the theoretical values obtained respectively by the lower and upper bounds. For very fine mesh of the numerical model of the footing (validation on a simple example of bearing capacity of a strip footing), the difference between Plaxis and Cast3M results is 7% (Table 2). This gap comes the difference between Drucker–Prager and Mohr–Coulomb materials. The analysis on the mesh density and element

type (TRI3 and TRI6) in Cast3M (Table 3) shows that, the difference between element type TRI3 and TRI6 results varies between 30 (for the very coarse mesh with local refinements under footing) to 0% (for the very fine mesh). The results of Table 3 show clearly that the element type, the mesh density and the convergence tolerances have a pronounced influence on the factor of safety obtained from the displacement finite-element method. Therefore, the influence of these parameters must be minimised by the use of high-order elements, very fine meshes and stringent tolerances in order to obtain a realistic results.

6.2. Retained walls–slope stability results

The Factor of Safety calculation procedure is based on the calculation of a stable initial stress and corresponding deformation state recursive reduction of the shear and tensile strength until a convergence to a prescribed tolerance is still obtainable. With regard to the retained walls–slope stability and backfill results at the phase 3.2 (part 5.4.3.2), the form of the failure surface obtained from Bishop and Janbu methods is very different from the other methods (Figure 26). The same is true for values of resulting safety factor (Table 5) which deviate from the value which taken for reference 1.55, against 1.89 for Bishop and 1.44 for Janbu. The Factor of Safety obtained by the FE methods (Cast3M, PLAXIS and TOCHNOG) is identical (1.56) and between the upper and lower bounds of OPTUM G2 (1.5 and 1.6). On the other hand, the value of 1.58 obtained by the Kinematic Element Method is an upper bounds and corresponds well to $1.55 + 0.03$ obtained by OPTUM G2 (Table 5). In view of these results, the Janbu method seems the most conservative. The difference in the results obtained is in agreement with the initial assumptions made for each method as follows.

- (a) For the limit equilibrium analysis, the need to guess the general form of the failure surface in advance makes it impossible to obtain a rigorous solutions. The poor choices giving poor estimates of the failure load. In practice, the correct form of the failure surface is often not intuitively obvious, especially for problems with an irregular geometry, complex loading, or complicated stratigraphy [32]. The resulting stresses do not satisfy equilibrium at every point in the domain. The analysis does not take into account the dilatancy of the materials and does not directly obtain the stresses and displacements in the structure. The failing soil mass is divided into slices for the calculation. The accuracy of the result depends on the width of each slice.
- (b) For the Kinematic Element Method, the theorem used is the approach of limit loads by upper bounds. It consists in constructing kinematics respecting boundaries conditions on displacements and in finding for each of them forces that are too great for the resistance of the soil [51]. This method overcomes the limits of the slice method in rigorous framework. It allows taking into account any geometries and stratigraphy, all flow conditions, point or distributed overloads in any direction and any type of reinforcement.
- (c) The finite-difference analysis is based in the explicit Lagrangian calculation scheme. The timestep of the calculation, the choice of the elements of the mesh and the numerical convergence have a pronounced influence on the factor of safety obtained from this method. Therefore, the influence of these parameters must be minimised by the use very small timestep of the calculation, convenient elements and stringent tolerances to obtain a realistic results.
- (d) The finite-element analysis is routinely applied for assessing displacements, stresses and strains for working load conditions, this technique is increasingly being used to calculate ultimate limit states and, consequently, factors of safety. In the finite-element codes the factor of safety is obtained by means of the strength reduction method; that is, an

analysis is performed with mobilised strength properties for the friction angle and the cohesion c , followed by an incremental decrease of $\tan\phi'$ and c' (assuming a Mohr–Coulomb failure criterion). This gives stress states that violate the strength criteria which are resolved in an iterative manner using the same stress point algorithm employed for a standard elasto-plastic analysis in finite-element codes, leading to a stress redistribution in the system until equilibrium can no longer be established and failure is reached [32]. However, close inspection of the developed failure mechanism and displacements of appropriate control points is required in order to avoid misinterpretation. It is well known that the element type, the mesh discretisation and the convergence tolerances have a pronounced influence on the factor of safety obtained from the displacement finite-element method. Therefore, the influence of these parameters must be minimised by the use of high-order elements, fine meshes and stringent tolerances in order to obtain a realistic results. Our numerical modelling were made using a very fine mesh in Cast3M models.

- (e) The new emerging method so-called finite-element limit analysis (FELA) is particularly powerful when both upper and lower bound estimates are calculated so that the true collapse load is bracketed from above and below. The difference between the two bounds then provides an exact measure of the error in the solution, and can be used to refine the meshes until a suitably accurate estimate of the collapse load is found [32].

The originality of our computation method is based on the adjustment of the factor FCUT allowing to regulate numerical gap between the very coarse mesh effect to very fine mesh of the model.

7. Conclusion

For geotechnical problems: Serviceability Limit State (SLS), computations are based on the deformation analysis. Ultimate Limit State (ULS): computations for stability analysis Strength reduction method are a powerful numerical technique implementing different safety concepts. It is argued that the Finite Element method of retaining wall and slope stability analysis is a more powerful alternative to traditional limit equilibrium methods and its widespread use should now be standard in geotechnical practice. Cast3M is an FE code dedicated mainly to the calculation of structures. At present, from a methodical, rigorous and sophisticated computation, we manage to solve complex geotechnical problems both at Serviceability Limit State (SLS) and the Ultimate Limit State analysis (ULS) by respecting the functional requirements and the different stages of construction allowing to have the overall stability which guarantees the durability of the geotechnical structure in comfortable safety conditions. The results presented in this paper were compared with those obtained by commercial industrial software dedicated to geotechnical problems and by reference solutions testifying to the reliability of our rigorous computation from the Cast3M code. A unique feature to Cast3M is the ability to compute rigorous factor of safety and analyses deliver adequate failure kinematics. The main contributions of this paper are the following:

- The implementation of a c - ϕ reduction procedure in Cast3M shows that this approach, which is often used as a black box in geotechnical softwares, can be implemented in rigorous way.
- The comparison with different methods commonly used in geotechnics shows that the implementation of c - ϕ reduction method is successful.
- The originality of the method is based on the adjustment of the factor FCUT allowing to regulate numerical gap between the very coarse mesh effect to very fine mesh of the model.

Declaration of interests

The authors confirm that there are no conflicts of interest associated with this publication and there has been no significant financial support for this work that could have influenced its outcome.

References

- [1] R. V. Whitman, W. A. Bailey, "Use of computers for slope stability analysis", *J. Soil Mech. Found. Div. ASCE* **93** (1967), no. SM4, p. 475-498.
- [2] D. V. Griffiths, P. Lane, "Slope stability analysis by finite elements", *Géotechnique* **49** (1999), no. 3, p. 387-403.
- [3] D. V. Griffiths, "Stability analysis of highly variable soils by elasto-plastic finite elements", Tech. report, Geomechanics Research Center, Colorado School of Mines, 2000.
- [4] D. V. Griffiths, "Stability analysis of highly variable soils by elasto-plastic finite elements", in *Advanced Numerical Applications and Plasticity in Geomechanics*, CISM, vol. 426, Springer, 2001, p. 159-229.
- [5] J. M. Duncan, "State of the art: limit equilibrium and finite-element analysis of slopes", *J. Geotech. Engng. ASCE* **122** (1996), no. 7, p. 577-596.
- [6] W. Fellenius, "Calculation of the stability of earth dams", in *Proceedings of the 2nd Congress on Large Dams, Engineering, Washington DC*, vol. 4, 1936, Corpus ID: 204624163.
- [7] A. W. Bishop, "The use of the slip circle in the stability analysis of slopes", *Geotechnique* **5** (1955), no. 1, p. 7-17.
- [8] J. Lowe, L. Karafiath, "Stability of earth dams upon drawdown", in *Proceedings of the 1st Pan-American Conference on Soil Mechanics and Foundation Engineering*, 1960, p. 537-552.
- [9] N. Janbu, "Slope stability computations", in *Soil Mechanics and Foundation Engineering Report*, Technical University of Norway, Trondheim, 1968.
- [10] N. R. Morgenstern, V. E. Price, "The analysis of the stability of general slip surfaces", *Geotechnique* **15** (1965), no. 1, p. 79-93.
- [11] N. R. Morgenstern, "Stability charts for earth slopes during rapid drawdown", *Geotechnique* **13** (1963), p. 121-131.
- [12] E. A. Spencer, "Method of analysis of the stability of embankments assuming parallel interslice forces", *Geotechnique* **17** (1967), no. 1, p. 11-26.
- [13] T. W. Lambe, F. Silva, "The ordinary method of slices revisited", *Geotech. News* **13** (1995), no. 3, p. 49-53.
- [14] I. M. Smith, R. Hobbs, "Finite element analysis of centrifuged and built-up slopes", *Geotechnique* **24** (1974), no. 4, p. 531-559.
- [15] D. W. Taylor, "Stability of earth slopes", *J. Boston Soc. Civ. Eng.* **24** (1937), p. 197-246.
- [16] O. C. Zienkiewicz, C. Humpheson, R. W. Lewis, "Associated and non-associated viscoplasticity and plasticity in soils mechanics", *Geotechnique* **25** (1975), no. 4, p. 671-689.
- [17] D. V. Griffiths, "Computation of bearing capacity factors using finite elements", *Géotechnique* **32** (1982), no. 3, p. 195-202.
- [18] D. V. Griffiths, "Computation of bearing capacity on layered soils", in *International Conference on Numerical Methods, Edmonton*, vol. 1, 1982, p. 163-170.
- [19] A. W. Bishop, N. R. Morgenstern, "Stability coefficients for earth slopes", *Geotechnique* **10** (1960), p. 129-150.
- [20] D. V. Griffiths, G. A. Fenton, "Probabilistic slope stability analysis by finite elements", *J. Geotech. Geoenviron. Eng.* **5** (2004), p. 507-518.
- [21] H. Chengya, Y. Leihua, S. Chenguang, N. Qihang, "Variational method for determining slope instability based on the strength reduction method", *Bull. Eng. Geol. Environ.* **81** (2022), no. 10, p. 1-12.
- [22] D. Anindita, K. S. Kumar, S. A. Rajib, "Numerical study on stability of soil slopes by limit equilibrium and finite element methods", in *National Level Conference on Engineering Problems and Application of Mathematics, NIT Agartala, June*, 2016.
- [23] R. W. Dakshith, D. Ashley, Y. Greg, K. Manoj, T. O. Ean, "Spatially variable coal slope stability analysis using image-based scaled boundary finite element method", in *15th World Congress on Computational Mechanics (WCCM-XV) and 8th Asian Pacific Congress on Computational Mechanics (APCOM-VIII), Virtual Congress: 31 July-5 August, 2022* (S. Koshizuka, ed.), 2022, 12 pages.
- [24] M. Huang, C.-Q. Jia, "Strength reduction FEM in stability analysis of soil slopes subjected to transient unsaturated seepage", *Comput. Geotech.* **36** (2009), no. 1-2, p. 93-101.
- [25] T. P. Huy, Z. O. Htet, J. Cheng, "Stability of slope and seepage analysis in earth dam using numerical finite element model", *Study of Civil Engineering and Architecture (SCEA)* **2** (2013), no. 4, p. 104-108.
- [26] S. H. Jiang, D. Q. Li, L. M. Zhang, C. B. Zhou, "Slope reliability analysis considering spatially variable shear strength parameters using a non-intrusive stochastic finite element method", *Eng. Geol.* **168** (2014), p. 120-128.
- [27] Z. Ambassa, J. C. Amba, J. C. Tchamba, "Modélisation et évaluation de la stabilité d'un talus renforcé par clouage industriel en utilisant la méthode c-phi reduction de Plaxis", *J. Afr. Sci.* **13** (2017), no. 1, p. 381-399.

- [28] A. Mouyexaux, C. Carvajal, P. Bressolette, L. Peyras, P. Breul, C. Bacconnet, "Probabilistic stability analysis of an earth dam by Stochastic Finite Element Method based on field data", *Comput. Geotech.* **101** (2019), p. 34-47.
- [29] K. Navid, Z. Annan, N. Majidreza, S. Shui-Long, "Improved prediction of slope stability using hybrid stacking ensemble method based on finite element analysis and field data", *J. Rock Mech. Geotech. Eng.* **13** (2021), p. 188-201.
- [30] Y. Yongtao, L. Feng, W. Wenan, "Assessing slope stability with an improved 3D numerical manifold method", *Rock Mech. Rock Eng. J.* **55** (2022), no. 10, p. 1-15.
- [31] F. S. Wong, "Uncertainties in FE modeling of slope stability", *Comput. Struct.* **19** (1984), p. 777-791.
- [32] S. W. Sloan, "Geotechnical stability analysis", *Geotechnique* **63** (2013), no. 7, p. 531-572.
- [33] F. Tschuchnigg, H. F. Schweiger, S. W. Sloan, A. V. Lyamin, I. Raissakis, "Comparison of finite-element limit analysis and strength reduction techniques", *Geotechnique* **65** (2015), no. 4, p. 249-257.
- [34] P. G. Fookes, "Tropical residual soils", in *Geological Society of London, Professional Handbooks*, Geological Society of London, 1997, ISBN-13: 978-1897799383. 184 pages.
- [35] Z. Ambassa, J. C. Amba, "Assessment of stiffness and strength parameters for the soft soil Model of clays of Cameroon", *Hindawi, Int. J. Adv. Civ. Eng.* **1** (2020), p. 1-16.
- [36] Z. Ambassa, J. C. Amba, F. X. Mbelen, "Monitoring and numerical modeling of the full-scale experimental embankment on soft Douala clays of Cameroon", *Int. J. Civil Eng. Technol.* **11** (2020), no. 7, p. 1-9.
- [37] P. Mestat, "Lois de comportement des géomatériaux et modélisation par la méthode des éléments finis", in *Etudes et recherches des Laboratoires Central des Ponts et Chaussées-série géotechnique (GT 52)*, Laboratoire Central des Ponts et Chaussées (LCPC), Paris, 1993, ISSN : 1157-3910. 139 pages.
- [38] A. J. Abbo, S. W. Sloan, "A smooth hyperbolic approximation to the Mohr-Coulomb yield criterion", *Comput. Struct.* **54** (1995), no. 3, p. 427-441.
- [39] O. C. Zienkiewicz, S. Valliappan, I. P. King, "Elasto-plastic solution of engineering problems, Initial stress, finite element approach", *Int. J. Numer. Methods Eng.* **1** (1969), p. 75-100.
- [40] C. S. Desai, "Overview, trends and projections: theory and application of the finite element method in geotechnical engineering", in *Proceedings of the Symposium Vicksburg, Mississippi, U.S. Army Engineer Waterways Experiment Station, January 1972* (C. S. Desai, ed.), vol. 1, Corps of Engineers, 1972, p. 3-90.
- [41] P. Mestat, P. Humbert, "Référentiel de tests pour la vérification de la programmation des lois de comportement dans les logiciels d'éléments finis", *Bull. laboratoires ponts chaussées* **230** (2001), p. 23-38.
- [42] D. M. Milovic, "Comparison between the calculated and experimental values of the ultimate bearing capacity", in *Proceedings, 6th International Conference on Soil Mechanics and Foundation Engineering, 8-15 September 1965*, vol. 2, University of Toronto Press, Montréal, 1965, p. 142-144.
- [43] V. V. Sokolovskij, *Statics of Soil Media*, Butterworths, London, 1960, Translated from the second Russian edition (1954) by D. H. Jones and A. N. Schofield, 237 pages.
- [44] K. Therzaghi, *Theoretical Soil Mechanics*, John Wiley, New York, 1943, 510 pages.
- [45] B. Simpson, "Finite elements applied to problems of plane strain deformation in soil", Phd thesis, Cambridge University, 1973.
- [46] R. De Borst, "Calculation of collapse loads using higher order elements", in *IUTAM Conference on Deformation and Failure of Granular Materials*, Balkema, Rotterdam, 1982, p. 503-513.
- [47] R. De Borst, P. Vermeer, "Possibilities and limitations of finite elements for limit analysis", *Geotechnique* **34** (1984), no. 2, p. 199-210.
- [48] R. De Borst, P. Vermeer, "Non-associated plasticity for soils", *Concr. Rock-Heron* **29** (1984), no. 3, p. 64.
- [49] R. Casciaro, L. Cascini, "Limit analysis by incremental-iterative procedure", in *IUTAM Conference on Deformation and Failure of Granular Materials*, Balkema, Rotterdam, 1982, p. 523-533.
- [50] G. L. Jiang, "Application de l'analyse limite à l'étude de la stabilité des massifs de sol", Thèse de doctorat ENPC, Paris, 1992.
- [51] J. Salençon, *Calcul à la rupture et analyse limite*, Presses de l'ENPC, Paris, 1983, 366 pages.
- [52] P. Mestat, "Validation du progiciel CESAR-LCPC en comportement mécanique non linéaire. Volume 1 : Fondations superficielles et tunnels", in *Rapport d'études et de recherches des Laboratoires des Ponts et des Chaussées, Série Géotechnique, GT 58*, 1994, ISSN 1157-3910. 179 pages.
- [53] J. T. Christian, A. J. Hagmann, W. A. Marr, "Incremental plasticity analysis of frictional soils", *Int. J. Numer. Anal. Method Geomech.* **1** (1997), no. 4, p. 343-375.
- [54] J. C. Nagtegaal, D. M. Parks, J. P. Rice, "On numerically accurate finite elements solutions in the fully plastic range", *Comput. Methods Appl. Mech. Eng.* **4** (1974), p. 153-177.
- [55] B. Hansen, N. H. Christensen, "Discussion of theoretical bearing capacity of very shallow footings", *J. Soil Mech. Found. Div. ASCE* **95** (1969), no. SM6, p. 1568-1572.
- [56] C. T. Toh, S. W. Sloan, "Finite element analyses of isotropic and anisotropic cohesive soils with a view to correctly predicting impending collapse", *Int. J. Numer. Anal. Methods Geomech.* **4** (1980), p. 1-23.

- [57] H. Van-Langen, P. A. Vermeer, "Automatic step size correction for non-associated plasticity problems", *Int. J. Numer. Methods Eng.* **29** (1990), p. 579-598.
- [58] C. S. Desai, H. J. Siriwardane, *Constitutive Laws for Engineering Materials with Emphasis on Geologic Materials*, Prentice Hall, Englewood Cliffs, NJ, 1984, ISBN 0-13-167940-6. 468 pages.
- [59] L. Jurgenson, "The application of theories of elasticity and plasticity to foundation problems", in *Contributions to Soil Mechanics 1925-1940*, Boston Society of Civil Engineers, ISSMGE 01-0036, Boston, MA, 1934.
- [60] H. J. Siriwardane, C. S. Desai, "Computational procedures for nonlinear three-dimensional analysis with some advanced constitutive laws", *Int. J. Numer. Anal. Methods Geomech.* **7** (1983), no. 2, p. 143-171.
- [61] S. W. Sloan, M. F. Randolph, "Numerical prediction of collapse loads using finite element methods", *Int. J. Numer. Anal. Methods Geomech.* **6** (1982), p. 47-76.
- [62] Cast3M-CEA[®], 2022, Cast3M is a research FEM code environment; its development is sponsored by the French Atomic Energy Commission, France, see web site: <http://www/cast3m.cea.fr/>.
- [63] A. S. Vesic, "Analysis of ultimate loads of shallow foundations", *J. Soil Mech. Found. Div. ASCE* **99** (1973), no. SM1, p. 45-73.
- [64] J. A. Brinch-Hansen, *General Formula for Bearing Capacity*, Danish Geotechnical Institute Bulletin 11, vol. 5, Copenhagen, and revue Ingeniøren, 1961, 38-46 pages.
- [65] J. A. Brinch-Hansen, *Revised and Extended Formula for Bearing Capacity*, Danish Geotechnical Institute Bulletin, vol. 28, 1970, 5-11 pages.
- [66] G. G. Meyerhof, "Some recent research on the bearing capacity of foundations", *Can. Geotech. J.* **1** (1963), no. 1, p. 16-26.
- [67] G. G. Meyerhof, *The Bearing Capacity and Settlements of Foundations*, Tech Press, 1982, ISBN-13: 978-0920692042.
- [68] PLAXIS[®], *Finite Element Code for Soil and Rock Analysis*, Material Models Manual, vol. 8, Brinkgreve, Delft University of Technology, 2018, 256 pages.
- [69] D. C. Drucker, "A more fundamental approach to plastic stress-strain analysis", in *Proceedings of the first UN National Congress of Applied Mechanics*, Division of Applied Mathematics, Brown University, USA, 1951, p. 487-491.
- [70] N. Tamaskovics, "Stability calculation with FEM with strength parameter reduction", *Geotechnik* **42** (2019), no. 2, p. 88-97.
- [71] G. T. R., "Guide des Terrassements Routiers, réalisation de remblais et des couches de forme", in *Fascicules I et II, SETRA-LCPC*, Ministère de l'Équipement, des Transport et du Tourisme, France, 2^e ed., 2000, p. 211.
- [72] D. M. Potts, L. Zdravkovic, *Finite Element Analysis in Geotechnical Engineering: Theory*, Thomas Telford Editors, 2001, ISBN-13: 978-0727727831, 444 pages.
- [73] R. B. Brinkgreve, "PLAXIS user's manual-Bentley: Finite Element Code for Soils and Rocks Analyses", 2021, <https://www.bentley.com>.
- [74] OPTUM G2[®], "Geotechnical analysis software-OptumCE: Finite Element Limit Analysis (FELA) Code for Soils and Rocks Analyses", 2022, <https://www.optumce.com>.
- [75] Talren v5[®], "Advanced slope stability analysis – Developed by Terrasol, France", 2020, <https://www.terrasol.fr>.
- [76] Tochnog[®], "Tochnog Professional software: Finite Element Program", in *GID User's Manual*, Tochnog Professional Company, 2022, <https://www.tochnogprofessional.nl>.
- [77] FLAC[®], "ITASCA International-Finite Differences code for Geotechnical Analyses", 2019, <https://www.itascainternational.com>.